

# Hybrid Forward Osmosis-Membrane Distillation System: Demonstration of Technical Feasibility

Linnet Zohrabian, Nicholas P. Hankins\*, Robert W. Field

*Department of Engineering Science, The University of Oxford, Parks Road, OX3 1PJ, Oxford, UK*

## Abstract

The hybridisation of forward osmosis (FO) and membrane distillation (MD) has the potential to offer a solution to the increasing worldwide demand for clean water. However, accurate prediction of system behaviour, balancing of water transfer rates and the implementation of a suitable draw solution are needed to maximise permeate production. Currently, there is a lack of comprehensive mathematical tools available and further draw solution developments are required. In this study, an experimentally validated mathematical model was developed to simulate the FO-MD system. Draw solutes including sodium chloride (NaCl), tetraethylammonium bromide (TEAB) and polydiallyldimethylammonium chloride (PDAC), were used to characterise individual FO and MD permeate fluxes. The FO-MD system was then run using 0.5 M NaCl, TEAB and PDAC. The results showed that fouling was more significant in FO, and water transfer rate imbalances were identified in all systems. The experimental results and model were used to predict MD feed temperature and cross-flow velocity adjustments to achieve system water balance for each draw solution. As a result of this balancing, permeate production using NaCl, TEAB and PDAC was enhanced. This study suggests that the FO-MD system is a promising candidate for water purification when system performance is optimised through mathematical modelling.

**Keywords:** Forward osmosis, Membrane distillation, Hybrid system, Mathematical modelling, Draw solution, Water transfer rate balancing

## 1. Introduction

In recent years, increasing shortages of clean water have presented a major concern for many countries around the world, with UNESCO estimating that 1.8 billion people could be residing in areas facing major water shortages by 2025 [1]. Desalination of seawater is an effective method for the production of clean water [2-4]. However, reverse osmosis (RO), currently the most widely used membrane technology for desalination, consumes relatively high quantities of energy, presents membrane fouling issues, and incurs high costs when operated at large scale [5, 6]. Hence, it is important that further research is conducted to find and develop competitive technology for water desalination that can meet the increasing demands for clean water in water-stressed communities around the world. In recent years, forward osmosis (FO) technology has attracted attention from many researchers [7-9]. FO is a process driven by an osmotic pressure gradient that is generated through the use of a draw solution. For operation to occur, the concentration of the draw solution must generate a greater osmotic pressure than that of the feed solution, resulting in a flow of water through the membrane. Since RO requires both pre-treatment and high hydraulic pressures, the potential benefits of FO include its ability to operate using low hydraulic pressures and potentially a reduced fouling propensity and lower energy requirements [10, 11].

There are numerous factors that can influence the performance and thus viability of the FO process for desalination at larger commercial scales. These factors can be linked to the characteristics of the FO membrane, the draw solution properties, the process operating conditions, including the resulting mass transfer coefficients, the long-term performance, life cycle assessment and cost estimation [12-18].

One challenge in particular is the need for further developments of draw solutions. During recent years, researchers have employed a wide variety of draw solutions for FO desalination, including inorganic and organic draw solutions, in order to investigate their effect on FO performance [19-23]. The ideal draw solution should generate high osmotic pressure and high permeate flux, show minimum draw solute reverse flux, allow ease of draw solution regeneration and exhibit minimum toxicity and cost. However, literature indicates that current draw solutions generally fall short of these traits and affect FO performance through low permeate fluxes, high reverse solute flux or draw solution recovery difficulties [7, 24, 25]. Achilli et al. [26] performed a series of experimental investigations on inorganic based draw solutions and developed a protocol for draw solution selection. It was shown that, for the same osmotic pressure (2.8 MPa), KCl generated the highest water flux, whilst  $\text{MgSO}_4$  resulted in the lowest reverse solute flux due to the larger size of the hydrated magnesium cation. Yen et al. [27] used a charged 2-methylimidazole based draw solution in a desalination process, achieving a permeate flux of 12 LMH after 6 hours of operation. However, a temperature of up to 70°C was required to recover the draw solute. Additionally, Zhao et al. [19] explored the use of a thermo-responsive copolymer, poly(sodium styrene-4-

---

\*Corresponding author.

E-mail address: nick.hankins@eng.ox.ac.uk (N.P. Hankins).

sulfonate-co-n-isopropylacrylamide) (PSSS-PNIPAM), as a draw solute for FO desalination. Using a feed solution of 0.6 M NaCl, permeate fluxes in excess of 3.5 LMH were observed for the PSSS-PNIPAM copolymer prepared with 15 wt% sodium-4-styrenesulfonate. Whilst PSSS-PNIPAM could be a promising draw solute for FO, it was suggested that further improvements are still required to maximise the osmotic pressures generated by thermo-responsive copolymers and reduce their viscosities.

Another challenge for FO is the need for improvements of the FO membrane. Whilst some studies have shown that FO membrane fouling is less severe and more reversible than for other membrane processes such as RO, fouling nonetheless remains a problem for the performance of FO [28-30]. The FO membrane should also favour the generation of high permeate fluxes and minimise concentration polarisation (CP). During CP, concentration boundary layers are formed outside and inside of the membrane and act to reduce the effective concentration gradient and thus osmotic driving force across the active layer of the membrane. Many experimental studies reported in the literature have been carried out using the cellulose triacetate (CTA) and thin film composite FO membranes manufactured by Hydration Technology Innovations (HTI) [8, 27, 31]. However, disruptions to the manufacturing of these membranes has limited the availability of commercial membranes for FO research. In addition to the release of new membranes from companies such as Aquaporin, several research groups have developed in-house FO membranes with varying degrees of success [32, 33].

Despite recent advances in FO draw solutions and membranes, another major barrier to the application of FO for large scale desalination operations is the coupling of FO with a suitable draw solution regeneration process. Several studies have investigated the use of membrane distillation (MD) as a regeneration process for FO desalination with promising results [6, 19, 34]. MD is a thermally-driven process that can separate water from a concentrated solution through the integration of a vapour permeation processes with a porous hydrophobic membrane. A major benefit of MD is its ability to separate solutions at lower temperatures than those used in conventional thermal technologies [35]. This makes MD suitable for utilising low-grade waste heat from natural gas compressor stations, power plants, or solar power, and this can contribute to cost savings [4, 36-38].

The FO-MD hybrid system has been investigated by desalination researchers and has a potential to respond to and meet the increasing challenge of widespread global shortages of clean water [6, 19, 34, 35]. Equipment in the hybrid FO-MD system is simple and easy to configure and energy requirements can be minimised [39-41]. A comprehensive review of hybrid FO systems carried out by Chekli et al. [41] highlighted the FO-MD system as a promising application for producing high quality water. However, their findings indicated that several limitations should be overcome before the process can become feasible at large scale. These include membrane pore wetting, a low feed recovery rate, uncertainty related to the availability of low-cost energy sources, and economic costs. A review of the hybrid FO-MD literature also indicates non-uniformity and non-accuracy of experimental results [41]. This could be due to the use of a large variety of feed and draw solutions, the short duration of experiments, the wide variety of membranes, and non-similar operating conditions. In addition, few studies have achieved balanced FO-MD water transfer rates [42-45]. Indeed, it appears that imbalances between the FO and MD sides of the system are not fully understood or addressed in the literature.

Numerous mathematical modelling studies have appeared in recent years predicting permeate flux through the FO membrane [46, 47]. Also previous work has investigated the effect of various feed and draw solution concentrations on the permeate flux through the FO membrane. Similarly, for MD, researchers have explored the impact of different operating parameters, such as feed temperature, on MD permeate flux [48, 49]. A literature review reveals only limited modelling work on predicting permeate flux with time as a function of operating conditions and membrane properties. Moreover, the lack of FO-MD hybrid system mathematical modelling has meant that few theoretical calculations have been performed to confirm experimental findings and identify measures to improve overall system performance. An FO-MD mathematical model can contribute to optimisation of the system configuration, selection of optimum operating conditions, and a control strategy for long-term system water balance. These benefits, in addition to the employment of a suitable membrane cleaning schedule, can help to maximise and sustain uniform permeate production, and minimise maintenance costs and process energy consumption.

The current study characterises an Aquaporin (AQP) Inside™ FO membrane using draw solutions including the surfactants TEAB and sodium dodecyl sulphate (SDS) and the polyelectrolyte PDAC. Few studies have investigated the effect of these draw solutions on FO-MD system performance, particularly with respect to time. Furthermore, imbalances between the FO and MD sides of the FO-MD hybrid system have frequently been identified in the literature. Therefore, both experimental and mathematical modelling are employed in this study to propose a suitable selection of parameters, in conjunction with a control strategy, to achieve balanced FO and MD water transfer rates. The modelling aspect of this study considers transfer processes within the FO and MD sides of the system, the influence of membrane fouling on system behaviour, and an analysis whereby optimisation of process operation and water transfer rate balancing could be achieved.

## 2. Development of FO-MD Mathematical Model

### 2.1. Forward Osmosis

The FO membrane possesses two inlet streams and two outlet streams for the entry and removal of the feed and draw solutions, respectively (Fig. 1). Considering  $x_{FO}$  as the coordinate in the direction of fluid flow, the overall feed side mass balance for a flat-sheet FO membrane is expressed by Eq. (1).

$$\frac{dQ_{FO,f}}{dx_{FO}} = J_{FO} w_{FO} \quad (1)$$

where  $Q_{FO,f}$  represents the feed flow rate,  $w_{FO}$  is the lateral width of the FO membrane and  $J_{FO}$  is the FO permeate flux. Accounting for volumetric continuity, Eq. (1) can be simplified to show that:

$$\frac{du_{FO,f}}{dx_{FO}} = \frac{J_{FO}}{h_{FO,f}} \quad (2)$$

where  $u_{FO,f}$  is the FO feed velocity and  $h_{FO,f}$  represents the FO feed channel height. Using Eq. (2), a component balance on the solute can be performed to determine changes in feed solute concentration,  $C_{FO,f}$ , in Eq. (3).

$$\frac{dC_{FO,f}}{dx_{FO}} = -\frac{J_S}{u_{FO,f}h_{FO,f}} - \frac{J_{FO}C_{FO,f}}{u_{FO,f}h_{FO,f}} \quad (3)$$

where  $J_S$  represents the FO reverse solute flux (RSF). Assuming the feed and draw solutes are the same species and counter-current flow, overall and component mass balances for the draw side of the FO membrane (denoted by the subscript d) lead to:

$$\frac{dQ_{FO,d}}{dx_{FO}} = J_{FO} w_{FO} \quad (4)$$

$$\frac{du_{FO,d}}{dx_{FO}} = \frac{J_{FO}}{h_{FO,d}} \quad (5)$$

$$\frac{dC_{FO,d}}{dx_{FO}} = -\frac{J_S}{u_{FO,d}h_{FO,d}} - \frac{J_{FO}C_{FO,d}}{u_{FO,d}h_{FO,d}} \quad (6)$$

The driving force behind FO is the osmotic pressure gradient formed through the application of the draw solution. The Van't Hoff equation can be applied for ideal cases, when osmotic pressure ( $\pi$ ) is linearly proportional to concentration. For concentrated feed or draw solutions, the osmotic pressure gradient is non-linear and the Van't Hoff equation leads to an inaccurate prediction of  $\pi$ . Hence, the Van't Hoff equation can be corrected by an osmotic pressure coefficient,  $\phi$  [50-52]:

$$\pi = \frac{\phi \beta R T C}{M_w} \quad (7)$$

where  $\beta$ ,  $R$ ,  $T$ ,  $C$  and  $M_w$  represent solute ionisation number, universal gas constant, absolute temperature, solution concentration and solute molecular weight, respectively. The osmotic pressure can also be related to the solute density number (Avogadro's number multiplied by the molar concentration of solute), with non-ideal solution behaviour modelled using the virial expansion [53, 54].

Fig. 1

Concentration polarisation (CP) can influence osmotic pressures generated by the draw and feed solutions. In the AL-FS (active layer-facing-feed solution) configuration, build-up of feed solute on the membrane surface leads to concentrative external concentration polarisation (ECP), as illustrated in Fig. 1, whilst dilutive internal concentration polarisation (ICP) emerges inside the membrane [55]. With the AL-DS (active layer-facing-draw solution) configuration, concentrative ICP, occurs when solute molecules accumulate at the SL-AL boundary (denoted by the concentration,  $C_i$ ). At the membrane exterior, the draw solution is diluted by permeate flux, leading to dilutive ECP (Fig. 1).

The FO permeate flux can be linked to the water permeability coefficient ( $A$ ), solute permeability coefficient ( $B$ ), system mass transfer coefficients and the osmotic pressures of the feed and draw solution [56]. To avoid the

use of an overall mass transfer coefficient, the AL-FS and AL-DS forms of the permeate flux equation, which consider the effects of CP, can be presented by Eqs. (8) and (9), respectively [18].

$$J_{FO} = A \left[ \pi_d \exp \left( -\frac{J_{FO}}{k_{sup}} \right) - \pi_f \exp \left( \frac{J_{FO}}{k_c} \right) \right] + B \left[ \exp \left( -\frac{J_{FO}}{k_{sup}} \right) - \exp \left( \frac{J_{FO}}{k_c} \right) \right] \quad (8)$$

$$J_{FO} = A \left[ \pi_d \exp \left( -\frac{J_{FO}}{k_c} \right) - \pi_f \exp \left( \frac{J_{FO}}{k_{sup}} \right) \right] + B \left[ \exp \left( -\frac{J_{FO}}{k_c} \right) - \exp \left( \frac{J_{FO}}{k_{sup}} \right) \right] \quad (9)$$

where  $k_{sup}$  represents the mass transfer coefficient for the channel adjacent to the AL and  $k_c$  is the mass transfer coefficient for the SL and its adjacent channel mass transfer coefficient (determined using the equations in Appendix A). These mass transfer coefficients can be related through Eq. (10).

$$\frac{1}{k_{sup}} = \frac{1}{k_c} + \frac{S}{D} \quad (10)$$

where  $D$  represents the diffusivity of solute in water and  $S$  is the structural parameter, which can be found using Eq. (11).

$$S = \frac{\delta_{FO} \tau_{FO}}{\varepsilon_{FO}} \quad (11)$$

where  $\delta_{FO}$ ,  $\tau_{FO}$  and  $\varepsilon_{FO}$  are the thickness, tortuosity and porosity of the support layer of the FO membrane, respectively.

With the known permeate flux,  $J_S$  can, assuming standard two parameter model is valid, be found using Eq. (12).

$$J_S = \frac{J_{FO} M_w B}{ANRT} \quad (12)$$

The above assumes that the reflection coefficient, which would be present in a three parameter model, is zero. With a three parameter model the ratio is no longer constant [57].

## 2.2. Membrane Distillation

The flow of MD feed (draw solution) along the length of the MD membrane, as presented by Fig. 2, can be expressed through an overall material balance, as shown by Eq. (13) which can also be simplified to Eq. (14) using the principle of continuity.

$$\frac{dQ_{MD,d}}{dx_{MD}} = -\frac{N_{MD} w_{MD}}{\rho} \quad (13)$$

$$\frac{du_{MD,d}}{dx_{MD}} = -\frac{N_{MD}}{\rho h_{MD,d}} \quad (14)$$

where  $Q_{MD,d}$ ,  $N_{MD}$  and  $w_{MD}$  are the MD feed flow rate, MD mass permeation flux and MD membrane internal width, respectively. The parameters  $u_{MD,d}$ ,  $h_{MD,d}$  and  $\rho$  are the MD feed solution velocity, MD feed solution channel height and solution density, respectively. The change in MD feed solution concentration along the membrane,  $C_{MD,d}$ , can be expressed by Eq. (15).

$$\frac{dC_{MD,d}}{dx_{MD}} = \frac{N_{MD} C_{MD,d}}{\rho u_{MD,d} h_{MD,d}} \quad (15)$$

For counter-current operation, a material balance on the MD permeate side (denoted by the subscript p), leads to:

$$\frac{dQ_{MD,p}}{dx_{MD}} = -\frac{N_{MD} w_{MD}}{\rho} \quad (16)$$

$$\frac{du_{MD,p}}{dx_{MD}} = -\frac{N_{MD}}{\rho h_{MD,p}} \quad (17)$$

Fig. 2.

The initial MD permeate flux in this study was determined using the modified Dusty Gas Model proposed by Field et al. [58] (Eq. (B.25), Appendix B).

The thermal boundary layers contribute to major MD flux reduction. The reduction in temperature gradient can be expressed by the so-called temperature polarisation coefficient,  $\theta$ , [18,59]:

$$\theta = \frac{T_{d,m} - T_{p,m}}{T_d - T_p} \quad (18)$$

where  $T_d$  and  $T_p$  state the bulk feed and permeate temperatures, respectively, and  $T_{d,m}$  and  $T_{p,m}$  are the temperatures of the feed and permeate at the membrane surface. The values of  $T_{d,m}$  and  $T_{p,m}$  cannot be measured directly and must be found through their relationship with other MD parameters [60].

Moreover, it should be noted that CP, represented by Eq. (19), can have greater influence at higher MD feed concentrations [59].

$$C_{MD,dm} = C_{MD,d} e^{(N_{MD}/\rho k_{MD})} \quad (19)$$

where  $k_{MD}$  is the MD mass transfer coefficient whilst  $C_{MD,d}$  and  $C_{MD,dm}$  are the concentrations of solute in the bulk feed solution and at the MD feed solution-membrane interface, respectively.

Other parameters needed to solve for the MD permeate flux can be determined using the equations shown in Appendix B.

### 2.3. Fouling Considerations

It is known that fouling can influence the behaviour of FO and MD permeate fluxes [35, 61, 62, 91]. NaCl can also contribute to membrane scaling, whereby particles are deposited onto the membrane surface, reducing the overall permeability [61]. To model the impact of scaling on FO, a logarithmic rate of fouling resistance,  $R_{sc}$ , has been proposed through Eq. (20).

$$R_{sc} = k_{sc1} \ln(k_{sc2}t + c_{sc}) \quad (20)$$

where  $k_{sc1}$ ,  $k_{sc2}$  and  $c_{sc}$  are system fouling constants that can be determined experimentally.

Adsorption of molecules onto the membrane surface is another mechanism through which solutes can reduce the FO permeate flux. In such instances, the permeate flux can decline quite rapidly over the initial operating period, which can be modelled through the following equation [63].

$$R_{ad} = k_{ad} t^{1/n_{ad}} \quad (21)$$

where  $R_{ad}$  is the rate at which molecules are adsorbed to the membrane surface, and the parameters  $k_{ad}$  and  $n_{ad}$  are system constants that represent the adsorption process during FO operation. Prior to fouling, the water permeability coefficient of the clean active layer,  $A_0$ , can be found using Eq. (22).

$$A_0 = \frac{1}{\mu R_{m,FO}} \quad (22)$$

where  $R_{m,FO}$  is the resistance of the clean FO membrane. With the onset of fouling, an additional resistance,  $R_f$ , should also be coupled with the resistance of the clean membrane:

$$A = \frac{1}{\mu(R_{m,FO} + R_f)} \quad (23)$$

where  $A$  represents the overall water permeability coefficient.

The FO literature makes frequent reference to 'A' and 'B' parameters. The equivalent terms herein are  $A_0$  and  $B$ .

The decline of MD permeate flux,  $J_{MD}$ , with time was determined using Eq. (B.26) [64], Appendix B.

## 2.4. Feed, Draw and Permeate Tank Material Balances

During FO-MD operation, the volume of feed solution in the FO feed tank,  $V_f$ , decreases over time due to the loss of permeate flux. Based on the conservation of fluid flow, the rate at which FO feed volume decreases can be defined by Eq. (24).

$$\frac{dV_f}{dt} = Q_{FO,f_{in}} - Q_{FO,f_{out}} \quad (24)$$

where  $Q_{FO,f_{in}}$  and  $Q_{FO,f_{out}}$  represent the FO feed flow rate entering and exiting the feed tank, respectively.

The feed concentration in the FO feed tank,  $C_f$ , is expected to increase with time due to the loss of permeate flux and generation of RSF. Accounting for these transfer processes, the rate of change of feed concentration can be expressed by Eq. (25).

$$\frac{dC_f}{dt} = \frac{1}{V_f} [C_{FO,f_{in}} Q_{FO,f_{in}} - C_f Q_{FO,f_{in}}] \quad (25)$$

where  $C_{FO,f_{in}}$  is the concentration of feed at entry to the feed tank.

Due to the hybrid nature of the FO-MD system, the draw solution volume in the draw tank,  $V_d$ , depends on both FO and MD properties, and can be represented by Eq. (26):

$$\frac{dV_d}{dt} = Q_{FO,d_{in}} + Q_{MD,d_{in}} - Q_{FO,d_{out}} - Q_{MD,d_{out}} \quad (26)$$

where  $Q_{FO,d_{in}}$  and  $Q_{FO,d_{out}}$  are the FO draw flow rates entering and exiting the draw tank, respectively, whilst  $Q_{MD,d_{in}}$  and  $Q_{MD,d_{out}}$  are the MD draw flow rates at the inlet and outlet of the draw tank, respectively.

The concentration of draw solution in the draw solution tank,  $C_d$ , is greatly influenced by the FO and MD permeate fluxes. A material balance on the draw solution tank leads to Eq. (27).

$$\frac{dC_d}{dt} = \frac{1}{V_d} [C_{FO,d_{in}} Q_{FO,d_{in}} + C_{MD,d_{in}} Q_{MD,d_{in}} - C_d Q_{FO,d_{in}} - C_d Q_{MD,d_{in}}] \quad (27)$$

where  $C_{FO,d_{in}}$  and  $C_{MD,d_{in}}$  represent the concentrations of draw solution at the outlet of the FO and MD membranes, respectively.

Re-concentration of the draw solution through MD will result in the generation of permeate flux. As a result, the increase in permeate volume,  $V_p$ , in the permeate collection tank is:

$$\frac{dV_p}{dt} = Q_{MD,p_{in}} - Q_{MD,p_{out}} \quad (28)$$

where  $Q_{MD,p_{in}}$  and  $Q_{MD,p_{out}}$  indicate the flow rates of MD permeate entering and exiting the permeate tank, respectively.

Further details on Eqs. (24)-(28) can be found in Appendix C.

In order to integrate and solve for the FO-MD mass balance equations, initial conditions were applied for each set of tests. The conditions that were used for the initial pre-balancing tests for NaCl, TEAB and PDAC draw solutions are presented in Table 1.

**Table 1**

As seen in Table 1, there are differences in the initial FO and MD permeate fluxes for each of the three draw solutions that were investigated. This is primarily due to differences in their properties, which is further explained in Sections 4.1 and 4.2.

## 3. Experimental Study

### 3.1. FO and MD membranes

The FO flat-sheet membrane used in this study was obtained from Aquaporin (Copenhagen, Denmark). According to the data provided by the manufacturer, the membrane has a thickness of 110  $\mu\text{m}$  and can be operated in temperature and pH ranges of 5-50°C and 2-11, respectively. The flat-sheet MD membrane, sourced from Membrane Solutions (MS) (Beijing, China), was used for the direct contact MD process. The membrane has a nominal pore size of 0.22  $\mu\text{m}$  and is composed of a poly(tetrafluoroethylene) active layer and a poly(propylene)

support layer. The main properties of the FO and MD membranes used in this study, in addition to those of the well-studied HTI CTA FO membrane, are presented in Table 2.

**Table 2**

### 3.2. Feed and Draw Solutions

Deionised (DI) water was used as the FO feed for the FO-MD experimental tests. During FO characterisation, a wide range of draw solutions were tested to investigate the behaviour of the system, including three organic draw solutes TEAB, SDS, and PDAC (Table 3). In particular, these three draw solutes were selected based on their different properties, such as molecular weights and charges, in addition to their promising performance in previous studies [8, 35].

**Table 3**

### 3.3. FO System, MD System and FO-MD Hybrid System

The desired fluid cross-flow velocities in the FO system were maintained using a peristaltic pump with two channels, obtained from Longer Pump (Taiwan). Individual FO tests were carried out using both AL-FS and AL-DS membrane configurations in order to determine the relationship between the draw solution concentration and FO permeate flux. The chemicals used to generate the draw solutions were purchased from Sigma Aldrich (UK). The change in feed and draw solution weights (and their volumes via the solution densities) were measured using a balance obtained from A&D Company Ltd. (Japan). The volume of water permeated through the membrane,  $\Delta V$ , was then used to find the experimental FO permeate flux using Eq. (29).

$$J_{FO} = \frac{\Delta V}{A_{FO} \Delta t} \quad (29)$$

where  $A_{FO}$  represents the effective area of the FO membrane.

**Fig. 3.**

The MD experimental configuration used in this study consisted of a peristaltic pump for the feed side of the process, which was purchased from Longer Pump (Taiwan), and a gear pump for the permeate side, obtained from Cole Parmer (USA). On the feed side, a water bath was used to maintain a constant feed water temperature to the MD test cell. Spacers were used on both sides of the membrane to generate turbulence and reduce TP and CP. An AL-FS membrane configuration and counter-current flow regime were used for MD. Moreover, both the MD feed inlet tubing and the test cell were insulated to minimise heat loss to the surroundings. To provide adequate cooling to the permeate stream, a cooler (Grant Instruments, Shepreth, UK) was set-up on the permeate side of MD. The feed and permeate temperatures were measured prior to entering MD using thermocouples. MD tests were conducted at various feed temperatures and cross-flow velocities, and the MD permeate flux was measured in a similar manner to that of the FO permeate flux.

The individual FO and MD processes were then combined to form a bench-scale FO-MD hybrid system, as shown in Fig. 3. In this process, the diluted draw solution from FO was continually re-concentrated through the MD process, prior to being recycled back into a common draw tank. Three draw solutions (NaCl, TEAB and PDAC) of 0.5 M concentration were selected for a series of FO-MD hybrid investigations. FO-MD hybrid tests were carried out using initial quantities of 0.4 L DI water in the permeate tank, 0.4 L of draw solution in the draw solution tank and 0.7 L of DI water in the FO feed tank. In each of the experiments, an AL-DS configuration was used for FO, whereas MD was operated using an AL-FS configuration. Prior to the start of the test runs, the system was operated to ensure that all solution temperatures met the specified initial set conditions. Between each test run, the FO and MD membranes were cleaned using a protocol which included acidic cleaning on the AL of the FO membrane and basic cleaning on the SL of the FO membrane and AL of the MD membrane [35]. For the initial testing phase, MD was run using feed and permeate temperatures of 30°C and 20°C, respectively. A cross-flow velocity of 0.2 m/s was maintained across the feed and draw sides of the FO membrane, as well as the feed side of the MD membrane giving Reynold numbers of the orders of  $10^2$  and  $10^3$  for FO and MD, respectively.

### 3.4. Optimisation of FO-MD Hybrid System using Model and Experimental Results

Following the initial run of FO-MD hybrid experimental tests, the model from Section 2 was used to optimise system performance. FO-MD hybrid system optimisation tests were then carried out using the new operating conditions identified. Since the effective area of the FO membrane in this study was greater than that of the MD membrane, matching the FO and MD permeate fluxes would not generate FO-MD system balance. Therefore, it was identified that comparison of the water transfer rates on both the FO and MD sides would provide a more useful insight into the balancing of the system. Considering equivalent units for the FO and MD permeate fluxes ( $J_{FO}$  and  $J_{MD}$ , respectively), the rate at which the draw solution is diluted through FO must be equal to the rate of re-concentration of the draw solution through MD, in order to operate a balanced system.

$$R_{t,FO} = J_{FO}A_{FO} \quad (30)$$

$$R_{t,MD} = J_{MD}A_{MD} \quad (31)$$

where  $R_{t,FO}$  and  $R_{t,MD}$  are the FO and MD water transfer rates, respectively, and  $A_{MD}$  is the effective area of the MD membrane.

## 4. Results and Discussion

### 4.1. Characterisation of FO Permeate Flux

The effect of draw solution concentration on FO permeate flux was investigated by using a range of inorganic and organic draw solutes. Amongst those considered, TEAB, SDS and PDAC were tested and their performances were compared with other common draw solutes, as shown in Fig. 4. The FO model was also applied and fitted to the experimental results (the fitting coefficients are presented in Table D1, Appendix D). The model is based upon the membrane specifications given in Table 2 and the equations provided in Section 2.1 and Appendix A.

Fig. 4.

The results in Fig. 4 show that increasing the concentration of each of the draw solutions leads to an increase in the FO permeate flux. This trend can be explained by the increasing osmotic pressure gradient across the membrane, which is apparent from Eq. (8) and Eq. (9). Membrane orientation is another factor that can influence FO permeate flux. The results in Fig. 4 reveal that the permeate fluxes generated in the AL-DS configuration are greater than those observed in the AL-FS configuration, which can be associated with the greater severity of the ICP effect in the AL-FS configuration. As shown by the experimental results and model prediction, the increase in permeate flux at lower draw solution concentrations is relatively linear. However, there is a noticeable reduction in the flux gradient at higher draw solution concentrations. This effect is more apparent in the AL-FS configuration, and prior work has shown that this trend occurs due to the flux limiting effect generated by ICP [9, 55].

The AQP membrane used in this study generates lower permeate fluxes in the AL-DS membrane configuration when compared to the HTI CTA membrane. At a draw solution concentration of 0.5 M, the experimental FO permeate fluxes are around 35.8%, 59.6% and 61.5% less than that of the HTI CTA membrane for NaCl, SDS and TEAB, respectively [35]. At the same molar concentration, these differences are reduced to around 23.1%, 17.9% and 58.5% when considering the AL-FS membrane configuration for NaCl, SDS and TEAB, respectively. It is likely that these trends arise due to the greater thickness of the AQP membrane, including that of the active layer, which could contribute to its lower membrane water permeability coefficient (Table 2) and therefore result in lower permeate fluxes [65].

Of the three organic draw solutes shown in Table 3, it is evident that TEAB produces the highest FO permeate flux at all tested draw solution concentrations and shows very similar performance to  $MgSO_4$  in the AL-DS configuration. This observation could be attributed to the lower molecular weight and lower viscosity of TEAB in solution, when compared to SDS and PDAC. As a result, these characteristics can lead to greater rates of mass transfer, and thus higher FO permeate fluxes across concentration polarisation boundary layers.

### 4.2. Characterisation of MD Permeate Flux

The MD permeate fluxes generated by 0.5 M of NaCl, TEAB and PDAC were measured at MD feed temperatures between 30-50°C, and are presented in Fig. 5 together with the model predictions calculated using Eq. (B.25), Appendix B.



**Fig. 5.**

The results show that there is an exponential increase in the MD permeate flux with feed temperature, as expected from inspection of Eq. (B.17), Appendix B, due to the resulting exponential increase in vapour pressure. In addition to influencing the solution properties such as diffusivity and viscosity, increasing the MD feed temperature can increase the fraction of energy that is used as the latent heat of vaporisation. This can therefore improve the thermal efficiency of the MD process (Eq. (B.24), Appendix B) [70-72]. However, studies have also shown that increasing the MD feed temperature can lead to greater temperature polarisation effects and more severe membrane fouling [73-76].

Fig. 5 reveals that the NaCl draw solution produced the highest MD permeate flux at each of the MD feed temperatures that were investigated, which could be due to its lower molecular weight, lower viscosity and higher diffusivity in solution. These properties can lead to a higher mass transfer coefficient and lower the effects of concentration polarisation.

It should be noted that MD feed temperatures within the range of 30-34.4°C were used for the FO-MD hybrid system experiments (Sections 4.3 and 4.4). To generate an initial set of permeate fluxes for FO-MD system testing, a lower temperature limit of 30°C was selected, which provided a temperature gradient of 10°C across the MD membrane. In addition, MD feed temperatures of up to 34.4°C were required to achieve FO-MD water transfer rate balancing.

#### *4.3. FO-MD Hybrid System Test Results*

**Fig. 6.**

The FO-MD hybrid system was operated for 10 hours using NaCl, TEAB and PDAC draw solutions at a concentration of 0.5 M, and the results of these tests are shown in Fig. 6. At this stage, only NaCl, TEAB and PDAC were selected from the initial set of draw solutions (Fig. 4) in order to represent different types of draw solutes with a range of molecular weights. The FO-MD hybrid system model was also used to simulate the experimental results. System fouling parameters, shown in Eqs. (20) and (21), were fitted for each of the three draw solutions; values are shown in Table 4.

**Table 4**

The results in Fig. 6 show that the adsorption model (Eq. 21) can be used to predict with reasonable accuracy the declining trend exhibited by the FO water transfer rates for TEAB and PDAC. Although the adsorption model can also be used to simulate the system with NaCl, Fig. 6a indicates that application of the scaling model used in this study leads to a better prediction of the FO water transfer rate achieved during the experiments. The difference in fouling behaviour for adsorption and scaling is also reflected in the rate at which the fouling resistance increases with time, as predicted by the FO-MD model in Fig. 7.

**Fig. 7.**

The pre-balancing test results shown in Fig. 6 reveal that the FO membrane exhibits a much greater tendency to foul in comparison with the MD membrane during the 10 hour test period. When considering the initial rate at which the FO water transfer rate declines, a more gradual decline is observed when the system is run with the NaCl draw solution compared to the other draw solutions. Between 10 minutes and 1 hour of operation, the FO water transfer rate for NaCl decreases by 16.9%; in contrast TEAB and PDAC show water transfer rate reductions of 19.4% and 41.5%, respectively, within the same time period. This supports the idea that the fouling behaviour and mechanism exhibited by the FO membrane is related to the type of draw solution used. These differences are also reflected in the apparent instantaneous increase in fouling resistance due to an adsorption mechanism (Fig. 7a), which is in contrast to the gradual increase that can be observed for a scaling resistance mechanism (Fig. 7b).

In addition, it is important to note that the membrane surface properties can also influence the initial rate at which the FO membrane fouls. This is supported through comparison of the FO water transfer rate declines experienced by the AQP and HTI CTA membranes under similar conditions. The results indicate that over the

first hour of operation, the reduction in the FO water transfer rate is around 4.1, 5.8 and 14.9 times greater for the AQP membrane using NaCl, TEAB and PDAC draw solutions, respectively, when compared to the HTI CTA membrane [35]. These differences could be linked to the higher surface roughness and relative hydrophobicity of the AQP membrane [65, 77], and appear to be further enhanced as the viscosity of the draw solution increases.

During the latter stages of operation, the results indicate that a limiting FO water transfer rate is achieved, whereby the rate of water transfer rate decline with time is much lower than that observed initially for the system. The presence of fouling in the FO system was supported by several experimental observations, including a change in colour of the FO membrane. Moreover, the FO water transfer rates in Fig. 6 were compared to the FO permeate fluxes (FO water transfer rate divided by FO membrane area) measured during the characterisation of the individual FO process (Fig. 4). This revealed that, after several hours of operation, the FO water transfer rates for NaCl, TEAB and PDAC in Fig. 6 were lower than the initial water transfer rates in Fig. 4. Further analysis showed that the NaCl draw solution was diluted from 0.5 M to 0.44 M after 10 hours. Under these conditions, it would be expected that the FO water transfer rate would decrease from around 0.025 L/hr to 0.023 L/hr, as a result of draw solution dilution. However, the actual FO water transfer rate decline measured during the 10 hour period was from 0.025 L/hr to 0.013 L/hr. These results therefore show that, whilst draw solution dilution does contribute to a slight decrease in the FO water transfer rate, a much larger proportion of the FO water transfer rate decline can be associated with FO membrane fouling. Similar observations were made for TEAB and PDAC, whose water transfer rate declines could also be predominantly attributed to fouling.

#### 4.4. FO-MD Hybrid System Balancing

The experimental results in Fig. 6 (left-hand side) also showed that there were imbalances in the water transfer rates for all three draw solutions between the FO and MD sides of the hybrid system. When considering pre-balancing experimental results, this trend is most significant for NaCl, with the FO water transfer rate after 1 hour approximately 2.3 times greater than that of MD. This is followed by TEAB and PDAC, with FO water transfer rates that are around 1.7 and 1.4 times larger than the MD water transfer rate, respectively. Moreover, from Fig. 6, it is evident the imbalances in water transfer rates continued to persist even after the decline in the FO water transfer rate due to draw solution dilution and membrane fouling. Whilst the results in this study have shown that the impact of draw solution dilution is relatively insignificant during the testing period of 10 hours (Section 4.3), differences in water transfer rates can have significant consequences over long periods of operation. Continued draw solution dilution can increase the MD water transfer rate, whilst the FO water transfer rate declines due to a reduction in the driving force across the membrane. This affords a natural balancing process; however, these processes can also accelerate the rate at which the MD membrane fouls, thus counter-acting the natural tendency of the system to balance [35]. As a result, it can become increasingly difficult to control the system and predict its long-term behaviour through mathematical modelling.

With this in mind, the FO-MD hybrid model was applied in order to balance the FO and MD water transfer rates. To maintain higher rates of water permeation in the FO-MD system, the operating parameters on the MD side of the system were adjusted to increase the magnitude of the MD water transfer rate. Using the model, it was seen that an FO-MD balance in the current system could be attained by judiciously increasing the temperature gradient across the MD membrane. This is supported by Fig. 5, which shows that MD is highly sensitive to changes in the feed temperature. Therefore, the MD feed temperature was selected as the primary control parameter for balancing the water transfer rates in the system.

However, throughout the experiments it was observed that the MD feed temperature experienced disturbances in practice that could not be eliminated through the programming of the water bath heating system. Thus, the MD cross-flow velocity was also selected as a secondary parameter to adjust during the tests, due to the ease of altering cross-flow velocity during system operation. The relationship between MD feed cross-flow velocity and the MD permeate flux was experimentally determined for NaCl, TEAB and PDAC, as shown in Fig. 8.

Fig. 8.

For each draw solution tested, Fig. 8 shows that increasing the cross-flow velocity results in a higher MD permeate flux. This can be explained by the increasing turbulence within the feed, which can disrupt the TP and CP external boundary layers and thus improve mass transfer within the MD process [49]. The overall effect of the MD feed side cross-flow velocity on the MD water transfer rate is less significant than that of the feed temperature (as observed by comparing Fig. 5 and Fig. 8). Nonetheless, between the draw solutions tested, varying MD feed cross-flow velocities within the range of 0.2-0.35 m/s was found to be sufficient in managing feed temperature disturbances and maintaining system balance (Table 5). In addition, MD feed temperature disturbances were more noticeable around the time at which the FO and MD water transfer rates were expected to balance. Therefore, the

MD feed cross-flow velocity was adjusted after 5 hours to reduce their effect on FO-MD water transfer rate balancing.

It should be noted that increasing the MD feed temperature for the purpose of achieving system balance will also affect the FO water transfer rate. At higher MD water transfer rates, the rate at which the draw solution is re-concentrated increases. In Section 4.3, it was shown that the overall contribution of draw solution dilution to the decline in the FO water transfer rate was lower than that due to fouling. However, its effect can be further minimised as a result of the higher MD water transfer rate, which can lead to an increase in the FO water transfer rate. Therefore, the final adjustment of MD cross-flow velocity should compensate for these additional effects, in addition to the disturbances in the MD feed temperature, in order to balance the system effectively.

Using the experimental unbalanced test results and the model, the values of both parameters (MD feed temperatures and cross-flow velocities) as required to achieve FO-MD system balance were identified. The experimental tests were then re-run using the determined MD feed temperatures and cross-flow velocities (Table 5), in order to achieve balanced FO-MD water transfer rates. The results of the balancing of NaCl, TEAB and PDAC systems are presented in Fig. 6 (right-hand side) and Table 6.

**Table 5**

The results in Fig. 6 indicate that controlled system balance is achieved within a shorter period of time than for natural system balancing, and particularly for PDAC (FO-MD balance was achieved after 2 hours). The rapid decline in the FO water transfer rate for PDAC, which appears to be a characteristic of adsorption fouling, could contribute to achieving FO-MD system balance within a shorter period of time. Moreover, the results suggest that, the FO-MD systems running with TEAB and PDAC can balance to generate more stable water transfer rates for a longer period of time within the 10 hour operating period (in comparison to the system with NaCl). Fig. 6d and Fig. 6f show that, upon system balance, the water transfer rates are exhibited after the fourth and second hours for TEAB and PDAC, respectively, are more constant. However, whilst a noticeable improvement in water transfer rate balancing is achieved for NaCl, the water transfer rates consistently decline after around three hours of operation. These observations could be linked to the different mechanisms by which FO membrane fouling occurs (related to the draw solution). Therefore, the rate at which the FO water transfer rate declines during the 10 hour testing period can also be attributed to progressive effects such as fouling. Since these results were obtained from short-term experiments (10 hours), additional long-term FO-MD tests can provide further insight into the areas of membrane fouling, ease of FO-MD system balancing and draw solution selection for the system.

In practical terms, the results for all three draw solutions show that a certain period of time is necessary before the FO and MD sides of the system are balanced. This period of time could be reduced through the implementation of an automated process control system. Process control can be used to detect water transfer rate imbalances due to factors such as membrane fouling, MD feed temperature disturbances and variations in the draw solution concentration. System parameters that require adjustment can then be selected and automatically applied to balance the FO and MD water transfer rates. Moreover, continual monitoring of the system and control of system balancing can also present benefits for long-term process operation for which manual adjustment of operating parameters may not be feasible.

The results in Table 6 reveal that, over the 10 hour period, system balancing results in an increase in permeate production for NaCl, TEAB and PDAC by 87.4%, 62.4% and 3.3% respectively, and is primarily due to the increase in MD feed operating conditions.

**Table 6**

It can also be observed that the system with NaCl shows the highest percentage increase in permeate production after 10 hours. However, the system with PDAC shows the greatest (35.5%) increase in MD permeate production relative to the water transfer rate generated through FO. This is due to a fall in the FO permeate flux, and could suggest the need for further optimisation of FO membrane cleaning when employing PDAC as a draw solution in the FO process.

## 5. Conclusions

This work highlights the role of experimental investigations and mathematical modelling in the design and operation of the FO-MD hybrid desalination system at large scale. In this study, a series of experiments were conducted to identify the influence of the main parameters in the FO and MD systems. In FO, a range of organic

and inorganic draw solutes were employed to measure the FO permeate flux at varying draw solution concentrations. Amongst the three organic draw solutes tested, TEAB generated the highest permeate flux due to its lower viscosity and higher solute diffusivity in solution. In MD, increasing the feed solution temperature led to an exponential increase in permeate flux for NaCl, TEAB and PDAC draw solutions. Running the FO-MD system for 0.5 M of NaCl, TEAB and PDAC draw solutions revealed that the FO membrane possessed a greater tendency to foul in comparison to the MD membrane over the 10 hour testing period. Selection of the MD feed temperature as the primary control parameter for balancing the water transfer rates in the system was successful.

The FO-MD hybrid model developed in this study was validated by FO and MD experimental results. Considering system fouling characteristics and water transfer rate imbalances, the model was then used to successfully predict the behaviour of the FO-MD system. Suitable control strategies were subsequently proposed, whereby the MD feed temperatures and cross-flow velocities were manually adjusted to achieve a system balance of water transfer rates, as required for long-term operation.

After achieving FO-MD system balance, permeate production for NaCl, TEAB and PDAC increased by 87.4%, 62.4% and 3.3% respectively over a period of 10 hours. The results from this study (Fig. 6) indicate that the FO-MD system shows optimum permeate production when FO and MD water transfer rates are balanced.

The results of the FO and MD water transfer rate balancing investigations indicate that the model is a useful tool that can be applied to improve understanding and performance of the system. However, manual adjustment of the MD operating parameters may not be sustainable over longer periods of operation. Thus, the FO-MD hybrid system will benefit from longer-term trials, the design and automation of an advanced process control system, and if required further refinement of the model.

## Appendix A. Calculation of parameters required to solve for FO permeate flux

The FO mass transfer coefficients (referred to in Section 2.1) can be determined through the use of the following empirical Sherwood correlations for the laminar and turbulent flow regimes [55, 78].

$$Sh = 0.04 (Re)^{0.75} (Sc)^{0.33} \quad \text{for } Re > 2100 \quad (A.1)$$

$$Sh = 1.85 \left( Re Sc \frac{H_{FO}}{x_{FO}} \right)^{0.33} \quad \text{for } Re < 2100 \quad (A.2)$$

where the parameters Sh, Re and Sc represent Sherwood, Reynolds and Schmidt numbers, respectively, and  $H_{FO}$  is the hydraulic diameter of the FO membrane, which can be determined separately for either side of the membrane using Eq. (A.3):

$$H_{FO} = \frac{2wh}{w+h} \quad (A.3)$$

Numerical values for the Reynolds and Schmidt numbers can be obtained through Eq. (A.4) and Eq. (A.5), respectively.

$$Re = \frac{\rho u H_{FO}}{\mu} \quad (A.4)$$

$$Sc = \frac{\mu}{\rho D} \quad (A.5)$$

Once the Sherwood number has been determined, Eq. (A.6) can be used to calculate the mass transfer coefficient.

$$k = \frac{ShD}{H_{FO}} \quad (A.6)$$

## Appendix B. Calculation of parameters required to solve for MD permeate flux

The temperatures of the draw and permeate solutions at the surface of the MD membrane can be determined using Eq. (B.1) and Eq. (B.2), respectively [79].

$$T_{d,m} = \frac{\frac{k_m}{\delta_{MD}} \left( T_p + \frac{h_d}{h_p} T_d \right) + h_d T_d - N_{MD} \Delta H_v}{\frac{k_m}{\delta_{MD}} + h_d \left( 1 + \frac{k_m}{\delta_{MD} h_p} \right)} \quad (B.1)$$

$$T_{p,m} = \frac{\frac{k_m}{\delta_{MD}}(T_d + \frac{h_p}{h_d}T_p) + h_p T_p + N_{MD} \Delta H_v}{\frac{k_m}{\delta_{MD}} + h_p \left(1 + \frac{k_m}{\delta_{MD} h_d}\right)} \quad (B.2)$$

where  $k_m$  and  $\delta_{MD}$  are the MD membrane thermal conductivity and thickness respectively, and  $\Delta H_v$ ,  $h_d$  and  $h_p$  represent the latent heat of vaporisation, and the draw and permeate solution heat transfer coefficients, respectively. The parameter  $k_m$  can be found using Isostress and Isostrain models, Eq. (B.3) and (B.4), respectively [80, 81].

$$k_m = \left[ \frac{\varepsilon_{MD}}{k_g} + \frac{(1-\varepsilon_{MD})}{k_s} \right]^{-1} \quad (B.3)$$

$$k_m = \varepsilon_{MD} k_g + (1 - \varepsilon_{MD}) k_s \quad (B.4)$$

where  $k_g$  and  $k_s$  are gas and polymer thermal conductivities, respectively. The value of  $k_s$  can be found using Eq. (B.5):

$$k_s = 4.86 \times 10^{-4} T_m + 0.253 \quad (B.5)$$

To calculate the heat transfer coefficients required in Eq. (B.1) and (B.2), a selection of correlations involving the Nusselt number can be employed [82, 83]:

$$Nu = 0.023(Re)^{0.8}(Pr)^{0.33} \quad \text{for } Re > 2100 \quad (B.6)$$

$$Nu = 1.86 \left( Re Pr \frac{H_{MD}}{h_{MD}} \right)^{0.33} \quad \text{for } Re < 2100 \quad (B.7)$$

where  $Pr$  represents the Prandtl number, which can be defined by Eq. (B.8):

$$Pr = \frac{\mu C_p}{k_c} \quad (B.8)$$

where  $C_p$  and  $k_c$  are fluid specific heat capacity and conductivity, respectively. The draw and permeate heat transfer coefficients can then be found using Eqs. (B.9) and (B.10):

$$h_d = \frac{Nu_d k_d}{H_{MD,d}} \quad (B.9)$$

$$h_p = \frac{Nu_p k_p}{H_{MD,p}} \quad (B.10)$$

where  $H_{MD,d}$ ,  $k_d$  and  $k_p$  represent the MD draw (feed) side hydraulic diameter and the thermal conductivities of the draw and permeate solutions, respectively. The latent heat of vaporisation must also be found using a suitable correlation, as shown by Eq. (B.11) [84]:

$$\Delta H_v = 1.7535 T_{d,m} + 2024.3 \quad (B.11)$$

Several parameters in Eq. (20) are determined prior to computation using MATLAB, as shown by Eq. (B.12) – (B.15) [57, 60, 84, 85].

$$D_{Kw} = \frac{d}{3} \sqrt{\frac{8RT_m}{\pi M_w}} \quad (B.12)$$

$$D_{w,a}^{P_T} = \frac{(1.895 \times 10^{-5}) T_m^{2.072}}{P_T} \quad (B.13)$$

$$\tau_{MD} = \frac{(2-\varepsilon_{MD})^2}{\varepsilon_{MD}} \quad (B.14)$$

$$Kn = \frac{l}{d} \quad (B.15)$$

where  $d$  and  $l$  represent the membrane pore size and mean free path, respectively. The mean free path can be found through Eq. (B.16), [60]:

$$l = \frac{k_b T_m}{\sqrt{2} \pi P_m (2.641 \times 10^{-10})^2} \quad (\text{B.16})$$

In addition, the air mole fractions at the draw and permeate-membrane interfaces appearing in Eq. (20) can be determined by considering the partial vapour pressures and the total membrane pressure. The partial vapour pressures of water at the draw and permeate sides can be estimated using the Antoine equation [60, 86]:

$$P_{w,d}^0 = e^{\left(23.20 - \frac{3816.44}{T_{d,m} - 46.13}\right)} \quad (\text{B.17})$$

$$P_{w,p}^0 = e^{\left(23.20 - \frac{3816.44}{T_{p,m} - 46.13}\right)} \quad (\text{B.18})$$

where  $P_{w,d}^0$  and  $P_{w,p}^0$  are the partial vapour pressures of water at the draw and permeate sides of the MD membrane, respectively. The presence of solute in the feed to the MD system will reduce both the vapour partial pressure and water flux in the system. Considering these effects, the draw solution partial vapour pressure can be corrected through Raoult's law [87].

$$P_w = P_{w,d}^0 (1 - x_s) \quad (\text{B.19})$$

where  $x_s$  is the mole fraction of solute in the feed.

The value of  $k_{MD}$  in Eq. (22) in Section 2.2. can be determined using suitable Sherwood correlations [88].

$$Sh = 0.023 Re^{0.8} Sc^{0.33} \quad \text{for } Re_d > 2100 \quad (\text{B.20})$$

$$Sh = 1.86 \left( Re Sc \frac{H_{MD,d}}{L} \right)^{1/3} \quad \text{for } Re_d < 2100 \quad (\text{B.21})$$

where  $L$  represents the length of the MD channel.

Moreover, in the direct contact MD process, heat transfer can be categorised into three stages: (i) heat transfer through the boundary layer of the feed (draw solution), (ii) heat transfer through the membrane and (iii) heat transfer through the boundary layer of the permeate stream.

In compliance with the conservation of energy, heat transferred through the membrane on the feed side is equivalent to the heat that passes through the permeate side. This idea can be extended to show that the heat transfer through the membrane is equal to the sum of latent heat that gives rise to evaporation,  $Q_v$ , and heat conduction through the membrane material,  $Q_c$  [81].

$$Q_v = N_{MD} \Delta H_v \quad (\text{B.22})$$

$$Q_c = \frac{k_m}{\delta} (T_{d,m} - T_{p,m}) \quad (\text{B.23})$$

The thermal efficiency,  $\eta_t$ , can therefore be written as:

$$\eta_t = \frac{Q_v}{Q_v + Q_c} \quad (\text{B.24})$$

The initial MD permeate flux in this study was determined using Eq. (B.25):

$$N_{MD} = \frac{(\epsilon_{MD}/\tau_{MD}) P_T (1 + Kn) D_{w,a}^{P_T}}{\delta_{MD} R T_m} \ln \left[ \frac{D_{Kw} y_{a,pm} + (1 + Kn) D_{w,a}^{P_T}}{D_{Kw} y_{a,dm} + (1 + Kn) D_{w,a}^{P_T}} \right] \quad (\text{B.25})$$

where  $\epsilon_{MD}$ ,  $\tau_{MD}$  and  $\delta_{MD}$  are the membrane porosity, tortuosity and thickness, respectively. The parameters  $P_T$ ,  $T_m$ ,  $D_{w,a}^{P_T}$ ,  $D_{Kw}$  and  $Kn$  state the total pressure, average membrane temperature, diffusion coefficients for ordinary and Knudsen diffusion and Knudsen number, respectively. The air mole fractions on the permeate and draw sides are represented by  $y_{a,pm}$  and  $y_{a,dm}$ , respectively.

Once the initial MD permeate flux is known, the change in MD permeate flux with time can also be calculated using Eq. (B.26).

$$J_{MD} = \frac{J_{MD0}}{a_0} e^{-\frac{3\rho_{MD,d}m_s c_m Q_{MD,d}}{2\rho_s d_s H_{MD,d} C_T^2 a_0} \left[ C_L e^{\frac{C_T}{\eta} \left( C_1 + \frac{t}{C_L} \right)} + \eta C_T C_{AT} \right]} - C_2 \quad (B.26)$$

where  $J_{MD0}$  and  $a_0$  represent the initial volumetric permeate flux and the initial membrane open pore area. The parameters  $m_s$ ,  $\rho_{MD,d}$  and  $\rho_s$ , are the draw mass fraction and densities of the draw solution and draw solute, respectively.  $H_{MD,d}$ ,  $d_s$ ,  $\eta$  and  $c_m$  are the MD draw side hydraulic diameter, draw solute diameter, friction coefficient and coefficient of deposited mass, respectively. The parameters  $C_T$ ,  $C_L$  and  $C_A$  are the stress coefficient, lubrication constant and system dependent constant respectively, whilst  $C_1$  and  $C_2$  are integration constants found during the derivation of Eq. (B.26).

## Appendix C. Feed, Draw and Permeate Tank Material Balances

Simplification of the material balance around the draw solution tank (Eq. 28, Section 4.2) leads to Eq. (C.1).

$$\frac{dV_d}{dt} = J_{FO} W_{FO} X_{FO} - \frac{N_{MD} W_{MD} X_{MD}}{\rho} \quad (C.1)$$

The material balance on the draw solute species in the draw tank (Eq. 29, Section 4.2) can also be simplified to show that:

$$\frac{dC_d}{dt} = \frac{1}{V_d} \left[ \left( \frac{C_d u_{FO,d0} h_{FO,d} - J_s X_{FO}}{u_{FO,d0} h_{FO,d} + J_{FO} X_{FO}} \right) (J_{FO} W_{FO} X_{FO} + u_{FO,d0} W_{FO} h_{FO,d}) + \left( \frac{u_{MD,d0} h_{MD,d} \rho C_d}{u_{MD,d0} h_{MD,d} \rho - N_{MD} X_{MD}} \right) \left( \frac{-N_{MD} W_{MD} X_{MD}}{\rho} + u_{MD,d0} W_{MD} h_{MD,d} \right) - C_d (J_{FO} W_{FO} X_{FO} + u_{FO,d0} W_{FO} h_{FO,d}) - C_d \left( \frac{-N_{MD} W_{MD} X_{MD}}{\rho} + u_{MD,d0} W_{MD} h_{MD,d} \right) \right] \quad (C.2)$$

where  $u_{FO,d0}$  and  $u_{MD,d0}$  represent the initial velocities of the FO and MD draw solution, and  $C_{FO,d0}$  indicates the initial concentration of the FO draw solution (at  $t=0$ ).

Similarly, the material balances for the concentration and volume of the feed solution in the feed tank, and the volume of the permeate in the permeate tank can also be derived and simplified to express FO-MD system and operating parameters.

It should be noted that constant permeates fluxes were assumed along the length of the FO and MD membranes. In this study, this assumption was justified due to the use of small FO and MD membrane lengths (10.5 cm and 9 cm, respectively), minimisation of polarisation effects through the application of the AL-DS configuration for FO, the employment of counter-current flow regimes for FO and MD, and the relatively short timescale of the investigations [12, 89, 90]. These factors, in conjunction with the accurate modelling predictions, can support the use of this assumption.

## Appendix D. Corrected Van't Hoff Factors

Table D1

### Nomenclature

#### Abbreviations

AL	Active layer
AQP	Aquaporin
CP	Concentration polarisation
CTA	Cellulose triacetate
DCMD	Direct contact membrane distillation
DI	De-ionised (water)
ECP	External concentration polarisation
FO	Forward osmosis
HTI	Hydration Technology Innovations
ICP	Internal concentration polarisation
MD	Membrane distillation
PDAC	Polydiallyldimethylammonium chloride
RO	Reverse osmosis
RSF	Reverse solute flux
SDS	Sodium dodecyl sulphate

SL	Support layer
TEAB	Tetraethylammonium bromide
TFC	Thin film composite
TP	Temperature polarisation

#### *Symbols*

A	Overall water permeability coefficient (L/m <sup>2</sup> h atm; L/m <sup>2</sup> h bar L/m <sup>2</sup> h Pa)
A <sub>0</sub>	Water permeability coefficient of clean membrane (L/m <sup>2</sup> h atm; L/m <sup>2</sup> h bar L/m <sup>2</sup> h Pa)
A <sub>FO</sub>	Effective FO membrane area (m <sup>2</sup> )
A <sub>MD</sub>	Effective MD membrane area (m <sup>2</sup> )
B	Solute permeability coefficient (m/s, L/m <sup>2</sup> h)
C	Solution concentration (kg/m <sup>3</sup> )
C <sub>A</sub>	System dependent constant (N/m)
C <sub>L</sub>	Lubrication constant (Pa s)
C <sub>p</sub>	Solution heat capacity (kJ/kg K)
C <sub>T</sub>	Stress coefficient of tangential force (Pa)
D	Diffusion coefficient (m <sup>2</sup> /s)
H	Hydraulic diameter (m)
H <sub>v</sub>	Latent heat of vaporisation (kJ/kg)
J <sub>FO</sub>	FO permeate flux (m/s; L/m <sup>2</sup> s; L/m <sup>2</sup> hr)
J <sub>MD</sub>	MD volumetric permeate flux (L/m <sup>2</sup> s; L/m <sup>2</sup> hr)
J <sub>s</sub>	Reverse solute flux (kg/m <sup>2</sup> s)
K	Solute resistivity (s/m)
Kn	Knudsen number
L	Membrane channel length (m)
M <sub>w</sub>	Molecular weight (kg/mol; g/mol)
N <sub>MD</sub>	MD mass permeation flux (kg/m <sup>2</sup> s)
Nu	Nusselt number
P	Pressure (Pa)
Pr	Prandtl number
Q	Solution flow rate (m <sup>3</sup> /s)
Q <sub>c</sub>	Heat transfer through conduction (W/m <sup>2</sup> )
Q <sub>m</sub>	Total heat transfer through membrane (W/m <sup>2</sup> )
Q <sub>v</sub>	Heat transfer through latent heat of vaporisation (W/m <sup>2</sup> )
R	Universal gas constant (m <sup>3</sup> atm/mol K; J/mol K)
R <sub>ad</sub>	Adsorption resistance (m <sup>-1</sup> )
R <sub>f</sub>	Fouling resistance (m <sup>-1</sup> )
R <sub>sc</sub>	Scaling resistance (m <sup>-1</sup> )
R <sub>t</sub>	Water transfer rate (L/hr)
Re	Reynolds number
T	Temperature (°C; K)
Sc	Schmidt number
Sh	Sherwood number
V	Tank volume (m <sup>3</sup> ; L)
a	Open pore area (m <sup>2</sup> )
c <sub>m</sub>	Coefficient of deposited mass
d	Membrane pore diameter (m)
d <sub>s</sub>	Solute diameter (m)
f	Friction coefficient
h	Membrane channel height (m)
h <sub>d</sub>	Draw heat transfer coefficient (W/m <sup>2</sup> K)
h <sub>p</sub>	Permeate heat transfer coefficient (W/m <sup>2</sup> K)
k	Mass transfer coefficient (m/s)
k <sub>b</sub>	Boltzmann constant (J/K; m <sup>2</sup> kg/s <sup>2</sup> K)
k <sub>d</sub>	Draw solution thermal conductivity (W/m K)
k <sub>g</sub>	Thermal conductivity of gas filling membrane pores (W/m K)
k <sub>m</sub>	Membrane thermal conductivity (W/m K)
k <sub>p</sub>	Permeate solution thermal conductivity (W/m K)
k <sub>s</sub>	Thermal conductivity of membrane material (W/m K)
l	Mean free path (m)
m <sub>s</sub>	Solid mass fraction



t	Time (s; hr)
u	Solution velocity (m/s)
w	Membrane width (m)
x	Membrane length (m)
$x_s$	Solid fraction
$y_a$	Air mole fraction

#### *Greek Symbols*

$\emptyset$	Osmotic pressure coefficient
$\alpha$	Aspect ratio
$\beta$	Ionisation number
$\Delta$	Change in parameter
$\delta$	Membrane thickness (m)
$\varepsilon$	Membrane porosity
$\zeta$	Concentration polarisation coefficient
$\eta$	MD friction coefficient
$\eta_t$	MD thermal efficiency
$\theta$	Temperature polarisation coefficient
$\mu$	Solution viscosity (Pa s)
$\pi$	Osmotic pressure (Pa, bar)
$\rho$	Solution density (kg/m <sup>3</sup> )
$\tau$	Membrane tortuosity
$\varphi$	Permeable surface parameter

#### *Subscripts*

0	Initial value of parameter
K	Knudsen
a	Air
ad	Adsorption
b	Bulk solution
c	Conductivity
d	Draw Solution
f	Feed Solution
g	Gas
m	Membrane
p	Permeate solution
s	Solute
sc	Scaling
w	Water

#### *Superscripts*

0	Standard state
---	----------------

## **Acknowledgments**

Linnet Zohrabian acknowledges the Department of Engineering Science at the University of Oxford for the award of an Engineering Science Doctoral Training Programme (EPSRC DTP) Studentship. During the period of this study RWF was partially supported by an APEX grant awarded by the Royal Society and British Academy and funded by the Leverhulme Trust.

## **References**

- [1] UNESCO, Managing Water under Uncertainty and Risk, The United Nations World Water Development Report 4, Vol. 1, 2012, <http://unesdoc.unesco.org/images/0021/002156/215644e.pdf>
- [2] M.A. García-Rubio, J. Guardiola, Desalination in Spain: A Growing Alternative for Water Supply, *International Journal of Water Resources Development* 28 (2012) 171-186.
- [3] M. Faigon, Success behind advanced SWRO desalination plant, *Filtration + Separation* 53 (3) (2016) 29-31, [https://doi.org/10.1016/S0015-1882\(16\)30121-5](https://doi.org/10.1016/S0015-1882(16)30121-5)
- [4] P.S. Goh, T. Matsuura, A.F. Ismail, N. Hilal, Recent trends in membranes and membrane processes for desalination, *Desalination* 391 (2016) 43-60, <https://doi.org/10.1016/j.desal.2015.12.016>
- [5] J. Su, R.C. Ong, P. Wang, T.-S. Chung, B.J., Helmer, J.S. de Wit, Advanced FO Membranes from Newly Synthesized CAP Polymer for Wastewater Reclamation through an Integrated FO-MD Hybrid System, *AIChE Journal* 59 (4) (2013) 1245-1254.

- [6] P. Wang, Y. Cui, Q. Ge, T.F. Tew, T.-S. Chung, Evaluation of hydroacid complex in the forward osmosis–membrane distillation (FO–MD) system for desalination, *Journal of Membrane Science* 494 (2015) 1–7, <https://doi.org/10.1016/j.memsci.2015.07.022>
- [7] Q. Ge, M. Ling, T.-S. Chung, Draw solutions for forward osmosis processes: Developments, Challenges, and Prospects for the future, *Journal of Membrane Science* 442 (2013) 225–237, <https://doi.org/10.1016/j.memsci.2013.03.046>
- [8] G. Gadelha, M.S. Nawaz, N.P. Hankins, S.J. Khan, R. Wang, C.Y. Tang, Assessment of micellar solutions as draw solutions for forward osmosis, *Desalination* 354 (2014) 97–106, <https://doi.org/10.1016/j.desal.2014.09.009>
- [9] Y.-N. Wang, R. Wang, W. Li, C.Y. Tang, Whey recovery using forward osmosis – Evaluating the factors limiting the flux performance, *Journal of Membrane Science* 533 (2017) 179–189, <https://doi.org/10.1016/j.memsci.2017.03.047>
- [10] B. Gu, D.Y. Kim, J.H. Kim, D.R. Yang, Mathematical model of flat sheet membrane modules for FO process: Plate-and-frame module and spiral-wound module, *Journal of Membrane Science* 379, (2011) 403–415, <https://doi.org/10.1016/j.memsci.2011.06.012>
- [11] N.A. Thompson, P.G. Nicoll, Forward Osmosis Desalination: A Commercial Reality, IDA World Congress – Perth Convention and Exhibition Centre (PCEC), Perth, Western Australia, Sept. 4–9, 2011.
- [12] T.Y. Cath, A.E. Childress, M. Elimelech, Forward osmosis: Principles, applications, and recent developments, *Journal of Membrane Science* 281 (2006) 70–87, <https://doi.org/10.1016/j.memsci.2006.05.048>
- [13] J. Su, S. Zhang, M.M. Ling, T.-S. Chung, Forward osmosis: an emerging technology for sustainable supply of clean water, *Clean Techn. Environ. Policy* 14 (4) (2012) 507–511.
- [14] P.G. Nicoll, Forward Osmosis - A Brief Introduction, Modern Water plc, The International Desalination Association World Congress on Desalination and Water Reuse, Tianjin, China, 2013.
- [15] R.V. Linares, Z. Li, S. Sarp, Sz.S. Buca, G. Amy, J.S. Vrouwenvelder, Forward osmosis niches in seawater desalination and wastewater reuse, *Water Research* 66 (2014) 122–139, <https://doi.org/10.1016/j.watres.2014.08.021>
- [16] L.C. Shen, N.P. Hankins, Forward Osmosis for Sustainable Water Treatment, Chapter 3 in: *Emerging Membrane Technology for Sustainable Water Treatment*, Elsevier, pp.55–76, 2016.
- [17] R.W. Field, J.J. Wu, Mass transfer limitations in forward osmosis: Are some potential applications overhyped?, *Desalination* 318 (2013) 118–124, <https://doi.org/10.1016/j.desal.2013.01.025>
- [18] R.W. Field, J.J. Wu, On boundary layers and the attenuation of driving forces in forward osmosis and other membrane processes, *Desalination* 429 (2018) 167–174, <https://doi.org/10.1016/j.desal.2017.12.001>
- [19] D. Zhao, P. Wang, Q. Zhao, N. Chen, X. Lu, Thermoresponsive copolymer-based draw solution for seawater desalination in a combined process of forward osmosis and membrane distillation, *Desalination* 348 (2014) 26–32, <https://doi.org/10.1016/j.desal.2014.06.009>
- [20] H.T. Nguyen, S.-S. Chen, N.C. Nguyen, H.H. Ngo, W. Guo, C.-W. Li, Exploring an innovative surfactant and phosphate-based draw solution for forward osmosis desalination, *Journal of Membrane Science* 489 (2015) 212–219, <https://doi.org/10.1016/j.memsci.2015.03.085>
- [21] Y. Cai, X.M. Hu, A critical review on draw solutes development for forward osmosis, *Desalination* 391 (2016) 16–29, <https://doi.org/10.1016/j.desal.2016.03.021>
- [22] R. Kumar, S. Al-Haddad, M. Al-Rughaib, M. Salman, Evaluation of hydrolyzed poly(isobutylene-alt-maleic anhydride) as a polyelectrolyte draw solution for forward osmosis desalination, *Desalination* 394 (2016) 148–154, <https://doi.org/10.1016/j.desal.2016.05.012>
- [23] J. Heo, K.H. Chu, N. Her, J. Im, Y.-G. Park, J. Cho, S. Sarp, A. Jang, M. Jang, Y. Yoon, Organic fouling and reverse solute selectivity in forward osmosis: Role of working temperature and inorganic draw solutions, *Desalination* 389 (2016) 162–170, <https://doi.org/10.1016/j.desal.2015.06.012>
- [24] H.K. Shon, L. Chekli, S. Phuntsho, J. Kim, J. Cho, Draw solutes in Forward Osmosis Processes, Chapter 5 in: *Forward Osmosis: Fundamentals and Applications*, American Society of Civil Engineers, pp.85–113, 2015.
- [25] H. Luo, Q. Wang, T.C. Zhang, T. Tao, A. Zhou, L. Chen, X. Bie, A review on the recovery methods of draw solutes in forward osmosis, *Journal of Water Process Engineering* 4 (2014) 212–223, <https://doi.org/10.1016/j.jwpe.2014.10.006>
- [26] A. Achilli, T.Y. Cath, A.E. Childress, Selection of inorganic-based draw solution for forward osmosis applications, *Journal of Membrane Science* 364 (2010) 233–241, <https://doi.org/10.1016/j.memsci.2010.08.010>
- [27] S.K. Yen, F.M. Haja N., M. Su, K.Y. Wang, T.-S. Chung, Study of draw solutes using 2-methylimidazole-based compounds in forward osmosis, *Journal of Membrane Science* 364 (2010) 242–252, <https://doi.org/10.1016/j.memsci.2010.08.021>
- [28] F.A. Siddiqui, Q. She, A.G. Fane, R.W. Field, Exploring the differences between forward osmosis and reverse osmosis fouling, *Journal of Membrane Science* 565 (2018) 241–253, <https://doi.org/10.1016/j.memsci.2018.08.034>
- [29] B. Mi, M. Elimelech, Organic fouling of forward osmosis membranes: fouling reversibility and cleaning without chemical reagents, *Journal of Membrane Science* 348 (2010) 337–345, <https://doi.org/10.1016/j.memsci.2009.11.021>
- [30] J.-J. Qin, W.C.L. Lay, K.A. Kekre, Recent developments and future challenges of forward osmosis for desalination: a review, *Desalin. Water Treat.* 39 (2012) 123–136.
- [31] N.C. Nguyen, H.T. Nguyen, S.-T. Ho, S.-S. Chen, H.H. Ngo, W. Guo, S.S. Ray, H.-T. Hsu, Exploring high charge of phosphate as new draw solute in a forward osmosis–membrane distillation hybrid system for concentrating high-nutrient sludge, *Science of the Total Environment* 557–558 (2016) 44–50, <https://doi.org/10.1016/j.scitotenv.2016.03.025>
- [32] P.M. Pardeshi, A.K. Mungray, A.A. Mungray, Polyvinyl chloride and layered double hydroxide composite as a novel substrate material for the forward osmosis membrane, *Desalination* 421 (2017) 149–159, <https://doi.org/10.1016/j.desal.2017.01.041>
- [33] M. Rastgar, A. Shakeri, A. Bozorg, S. Salehi, V. Saadattalab, Highly-efficient forward osmosis membrane tailored by magnetically responsive graphene oxide/Fe<sub>3</sub>O<sub>4</sub> nanohybrid, *Applied Surface Science* 441 (2018) 923–935, <https://doi.org/10.1016/j.apsusc.2018.02.118>
- [34] Y.-N. Kwon, M.-J. Kim, Y.T. Lee, Application of a FO/MD-combined system for the desalination of saline solution, *Desalination and Water Treatment* 57 (2016) 14347–14354.
- [35] F. Parveen, Development of Lab-scale Forward Osmosis Membrane Bioreactor (FO-MBR) with Draw Solute Regeneration for Wastewater Treatment, DPhil Thesis, University of Oxford, UK, 2018.
- [36] H.C. Duong, P. Cooper, B. Nelemans, T.Y. Cath, L.D. Nghiem, Optimising thermal efficiency of direct contact membrane distillation by brine recycling for small scale seawater desalination, *Desalination* 374 (2015) 1–9, <https://doi.org/10.1016/j.desal.2015.07.009>
- [37] N. Dow, S. Gray, J.-D. Li, J. Zhang, E. Ostarcevic, A. Liubinas, P. Atherton, G. Roeszler, A. Gibbs, M. Duke, Pilot trial of membrane distillation driven by low grade waste heat: Membrane fouling and energy assessment, *Desalination* 391 (2016) 30–42, <https://doi.org/10.1016/j.desal.2016.01.023>
- [38] O.R. Lokare, S. Tavakkoli, G. Rodriguez, V. Khanna, R.D. Vidic, Integrating membrane distillation with waste heat from natural gas compressor stations for produced water treatment in Pennsylvania, *Desalination* 413 (2017) 144–153, <https://doi.org/10.1016/j.desal.2017.03.022>
- [39] S. Zhao, L. Zou, C.Y. Tang, D. Mulcahy, Recent developments in forward osmosis: Opportunities and challenges, *Journal of Membrane Science* 396, (2012) 1–21, <https://doi.org/10.1016/j.memsci.2011.12.023>

- [40] P. Nasr, H. Sewilam, The potential of groundwater desalination using forward osmosis for irrigation in Egypt, *Clean Techn. Environ. Policy* 17 (7) (2015) 1883-1895.
- [41] L. Chekli, S. Phuntsho, J.E. Kim, J. Kim, J.Y. Choi, J.-S. Choi, S. Kim, J.H. Kim, S. Hong, J. Sohn, H.K. Shon, A comprehensive review of hybrid forward osmosis systems: Performance, applications and future prospects, *Journal of Membrane Science* 497 (2016) 430-449, <https://doi.org/10.1016/j.memsci.2015.09.041>
- [42] Q. Ge, P. Wang, C. Wan, T.-S. Chung, Polyelectrolyte-Promoted Forward Osmosis-Membrane Distillation (FO-MD) Hybrid Process for Dye Wastewater Treatment, *Environ. Sci. Technol.* 46 (2012) 6236-6243.
- [43] K.Y. Wang, M.M. Teoh, A. Nugroho, T.-S. Chung, Integrated forward osmosis-membrane distillation (FO-MD) hybrid system for the concentration of protein solutions, *Chemical Engineering Science* 66 (2011) 2421-2430, <https://doi.org/10.1016/j.ces.2011.03.001>
- [44] T. Husnain, Y. Liu, R. Riffat, B. Mi, Integration of forward osmosis and membrane distillation for sustainable wastewater reuse, *Separation and Purification Technology* 156 (2015b) 424-431, <https://doi.org/10.1016/j.seppur.2015.10.031>
- [45] Y. Zhou, M. Huang, Q. Deng, T. Cai, Combination and performance of forward osmosis and membrane distillation (FO-MD) for treatment of high salinity landfill leachate, *Desalination* 420 (2017) 99-105, <https://doi.org/10.1016/j.desal.2017.06.027>
- [46] S.-M. Shim, W.-S. Kim, A numerical study on the performance prediction of forward osmosis process, *Journal of Mechanical Science and Technology* 27 (4) (2013) 1179-1189.
- [47] D.Y. Kim, B. Gu, D.R. Yang, An explicit solution of the mathematical model for osmotic desalination process, *Korean J. Chem. Eng.*, 30 (9) (2013) 1691-1699.
- [48] A. Alkhdhiri, N. Darwish, N. Hilal, Membrane distillation: A comprehensive review, *Desalination* 287 (2011) 2-18, <https://doi.org/10.1016/j.desal.2011.08.027>
- [49] Y.M. Manawi, M. Khraisheh, A.K. Fard, F. Benyahia, S. Adham, Effect of operational parameters on distillate flux in direct contact membrane distillation (DCMD): Comparison between experimental and model predicted performance, *Desalination* 336 (2014) 110-120, <https://doi.org/10.1016/j.desal.2014.01.003>
- [50] M. Park, J.J. Lee, S. Lee, J.H. Kim, Determination of a constant membrane structure parameter in forward osmosis processes, *Journal of Membrane Science* 375 (2011) 241-248, <https://doi.org/10.1016/j.memsci.2011.03.052>
- [51] N.M. Mazlan, Forward Osmosis for Desalination and Water Recovery, PhD Thesis, Imperial College London, UK, 2016.
- [52] D.J. Johnson, W.A. Suwaileh, A.W. Mohammed, N. Hilal, Osmotic's potential: An overview of draw solutes for forward osmosis, *Desalination* 434 (2018) 100-120, <https://doi.org/10.1016/j.desal.2017.09.017>
- [53] A. Yokozeki, Osmotic pressures studied using a simple equation-of-state and its applications, *Applied Energy* 83 (2006) 15-41, <https://doi.org/10.1016/j.apenergy.2004.10.015>
- [54] M. Qasim, N.A. Darwish, S. Sarp, N. Hilal, Water desalination by forward (direct) osmosis phenomenon: A comprehensive review, *Desalination* 374 (2015) 47-69, <https://doi.org/10.1016/j.desal.2015.07.016>
- [55] J.R. McCutcheon, M. Elimelech, Influence of concentrative and dilutive internal concentration polarization on flux behavior in forward osmosis, *Journal of Membrane Science* 284 (2006) 237-247, <https://doi.org/10.1016/j.memsci.2006.07.049>
- [56] S. Loeb, L. Titelman, E. Korngold, J. Freiman, Effect of porous support fabric on osmosis through a Loeb-Sourirajan type asymmetric membrane, *Journal of Membrane Science* 129 (2) (1997) 243-249, [https://doi.org/10.1016/S0376-7388\(96\)00354-7](https://doi.org/10.1016/S0376-7388(96)00354-7)
- [57] J.J. Wu, On the application of the Spiegler-Kedem model to forward osmosis, *BMC Chemical Engineering* (2019) 1:15.
- [58] R.W. Field, H.Y. Wu, J.J. Wu, Multiscale modeling of membrane distillation: Some theoretical considerations, *Ind. Eng. Chem. Res.* 52 (26) (2013) 8822-8828.
- [59] L. Martínez-Díez and M.I. Vázquez-González, Effects of Polarization on Mass Transport through Hydrophobic Porous Membranes, *Ind. Eng. Chem. Res.* 37 (10) (1998) 4128-4135.
- [60] M. Khayet, Membranes and theoretical modeling of membrane distillation: A review, *Advances in Colloid and Interface Science* 164 (2011) 56-88, <https://doi.org/10.1016/j.cis.2010.09.005>
- [61] E. Drioli, A. Ali, F. Macedonio, Membrane Distillation: Recent developments and perspectives, *Desalination* 356 (2015) 56-84, <https://doi.org/10.1016/j.desal.2014.10.028>
- [62] Y. Chun, D. Mulcahy, L. Zou, I.S. Kim, A Short Review of membrane Fouling in Forward Osmosis Processes, *Membranes* 7 (2) 30 (2017) <https://doi.org/10.3390/membranes7020030>
- [63] H.K. Shon, S. Vigneswaran, J. Kandasamy, W.G. Shim, Ultrafiltration Of Wastewater with Pretreatment: Evaluation Of Flux Decline Models, *Desalination* 231 (2008) 332-339, <https://doi.org/10.1016/j.desal.2007.10.035>
- [64] M. Ramezani-pour, M. Sivakumar, An analytical flux decline model for membrane distillation, *Desalination* 345 (2014) 1-12, <https://doi.org/10.1016/j.desal.2014.04.006>
- [65] L. Xia, M.F. Andersen, C. Hélix-Nielsen, J.R. McCutcheon, Novel Commercial Aquaporin Flat-sheet Membrane for Forward Osmosis, *Industrial & Engineering Chemistry Research* 56 (41) (2017) 11919-11925.
- [66] J. Ren and J.R. McCutcheon, A new commercial thin film composite membrane for forward osmosis, *Desalination* 343 (2014) 187-193, <https://doi.org/10.1016/j.desal.2013.11.026>
- [67] M. Xie, L.D. Nghiem, W.E. Price, M. Elimelech, Relating rejection of trace organic contaminants to membrane properties in forward osmosis: Measurements, modelling and implications, *Water Research* 49 (2014) 265-274, <https://doi.org/10.1016/j.watres.2013.11.031>
- [68] C.Y. Tang, Q. She, W.C.L. Lay, R. Wang, A.G. Fane, Coupled effects of internal concentration polarization and fouling on flux behavior of forward osmosis membranes during humic acid filtration, *Journal of Membrane Science* 354 (2010) 123-133, <https://doi.org/10.1016/j.memsci.2010.02.059>
- [69] Membrane Solutions, 2019, <https://www.membrane-solutions.com>
- [70] J. Zhang, N. Dow, M. Duke, E. Ostarcevic, J.-D. Li, S. Gray, Identification of material and physical features of membrane distillation membranes for high performance desalination, *Journal of Membrane Science* 349 (2010) 295-303, <https://doi.org/10.1016/j.memsci.2009.11.056>
- [71] J. Zhang, S. Gray, J.-D. Li, Predicting the influence of operating conditions on DCMD flux and thermal efficiency for incompressible and compressible membrane systems, *Desalination* 323 (2013) 142-149, <https://doi.org/10.1016/j.desal.2013.04.002>
- [72] R. Ullah, M. Khraisheh, R.J. Esteves, J.T. McLeskey Jr, M. AlGhouti, M. Gad-el-Hak, H.V. Tafreshi, Energy efficiency of direct contact membrane distillation, *Desalination* 433 (2018) 56-67, <https://doi.org/10.1016/j.desal.2018.01.025>
- [73] L.M. Camacho, L. Dumée, J. Zhang, J. Li, M. Duke, J. Gomez, S. Gray, Advances in Membrane Distillation for Water Desalination and Purification Applications, *Water* 5 (2013) 94-196.
- [74] J. Ge, Y. Peng, Z. Li, P. Chen, S. Wang, Membrane fouling and wetting in a DCMD process for RO brine concentration, *Desalination* 344 (2014) 97-107, <https://doi.org/10.1016/j.desal.2014.03.017>
- [75] L.D. Tijting, Y.C. Woo, J.-S. Choi, S. Lee, S.-H. Kim, H.K. Shon, Fouling and its control in membrane distillation – A review, *Journal of Membrane Science* 475 (2015) 215-244, <https://doi.org/10.1016/j.memsci.2014.09.042>
- [76] J. Zhang, N. Dow, M. Duke, E. Ostarcevic, J.-D. Li, S. Gray, Identification of material and physical features of membrane distillation membranes for high performance desalination, *Journal of Membrane Science* 349 (2010) 295-303, <https://doi.org/10.1016/j.memsci.2009.11.056>

- [77] Y. Chun, L. Qing, G. Sun, M.R. Bilad, A.G. Fane, T.H. Chong, Prototype aquaporin-based forward osmosis membrane: Filtration properties and fouling resistance, *Desalination* 445 (2018) 75-84, <https://doi.org/10.1016/j.desal.2018.07.030>
- [78] C.H. Tan, H.Y. Ng, Modified models to predict flux behavior in forward osmosis in consideration of external and internal concentration polarizations, *Journal of Membrane Science* 324 (2008) 209-219, <https://doi.org/10.1016/j.memsci.2008.07.020>
- [79] M. Khayet, A. Velázquez, J.I. Mengual, Modelling mass transport through a porous partition: Effect of pore size distribution, *J. Non-Equilib. Thermodyn.* 29 (2004) 279-299.
- [80] J. Phattaranawik, R. Jiratananon, A.G. Fane, Heat transport and membrane distillation coefficients in direct contact membrane distillation, *Journal of Membrane Science* 212 (2003) 177-193, [https://doi.org/10.1016/S0376-7388\(02\)00498-2](https://doi.org/10.1016/S0376-7388(02)00498-2)
- [81] R.W. Schofield, A.G. Fane, C.J.D. Fell, Heat and mass transfer in membrane distillation, *Journal of Membrane Science* 33 (1987) 299-313.
- [82] L. Martínez-Díez, M.I. Vázquez-González, Temperature and concentration polarization in membrane distillation of aqueous salt solutions, *Journal of Membrane Science* 156 (2) (1999) 265-273, [https://doi.org/10.1016/S0376-7388\(98\)00349-4](https://doi.org/10.1016/S0376-7388(98)00349-4)
- [83] S. Srisurichan, R. Jiratananon, A.G. Fane, Mass transfer mechanisms and transport resistances in direct contact membrane distillation process, *Journal of Membrane Science* 277 (2006) 186-194, <https://doi.org/10.1016/j.memsci.2005.10.028>
- [84] H.Y. Wu, Direct Contact Membrane Distillation: Analysis and Application, DPhil Thesis, University of Oxford, UK, 2015.
- [85] J. Phattaranawik, R. Jiratananon, A.G. Fane, Effect of pore size distribution and air flux on mass transport in direct contact membrane distillation, *Journal of Membrane Science* 215 (2003) 75-85, [https://doi.org/10.1016/S0376-7388\(02\)00603-8](https://doi.org/10.1016/S0376-7388(02)00603-8)
- [86] K.W. Lawson, D.R. Lloyd, Membrane distillation, *Journal of Membrane Science* 124 (1997) 1-25.
- [87] M. Qtaishat, T. Matsuura, B. Kruczek, M. Khayet, Heat and mass transfer analysis in direct contact membrane distillation, *Desalination* 219 (2008) 272-292, <https://doi.org/10.1016/j.desal.2007.05.019>
- [88] Y. Yun, R. Ma, W. Zhang, A.G. Fane, J. Li, Direct contact membrane distillation mechanism for high concentration NaCl solutions, *Desalination* 188 (2006) 251-262, <https://doi.org/10.1016/j.desal.2005.04.123>
- [89] J. Lee, B. Kim, S. Hong, Fouling distribution in forward osmosis membrane process, *Journal of Environmental Sciences*, 26 (6) (2014) 1348-1354, [https://doi.org/10.1016/S1001-0742\(13\)60610-5](https://doi.org/10.1016/S1001-0742(13)60610-5)
- [90] J. Korak, M. Arias-Paic, Forward Osmosis Evaluation and Applications for Reclamation, U.S. Department of the Interior Bureau of Reclamation Technical Service Center, Denver, Colorado, USA, 2015.
- [91] T.-T. Nguyen, S. Kook, C. Lee, R.W. Field, I.S. Kim, Critical flux-based membrane fouling control of forward osmosis: Behavior, sustainability, and reversibility, *Journal of Membrane Science* 570-571 (2019) 380-393, <https://doi.org/10.1016/j.memsci.2018.10.062>

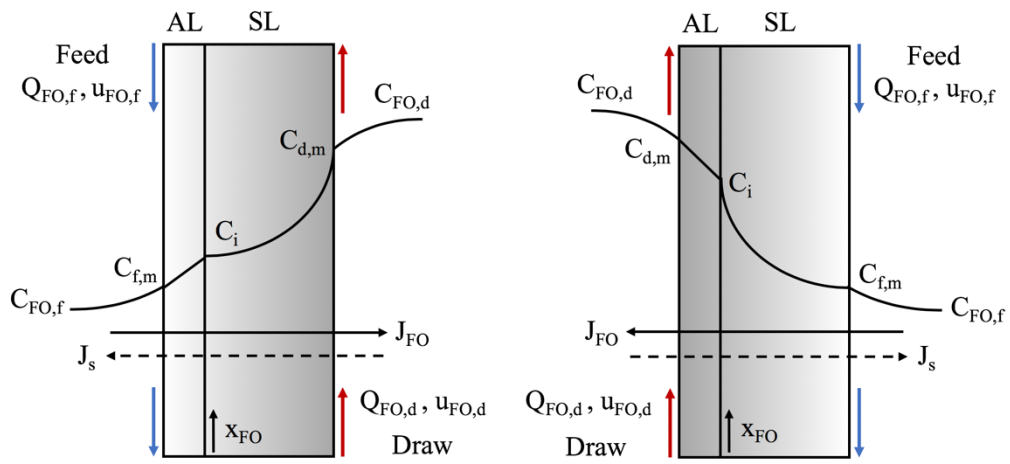


**Fig. 1.** Illustration of concentration polarisation in (a) AL-FS FO membrane configuration and (b) AL-DS FO membrane configuration

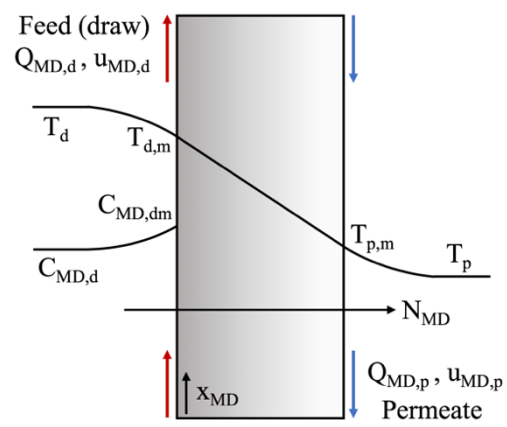


**Fig. 2.** Schematic of MD membrane

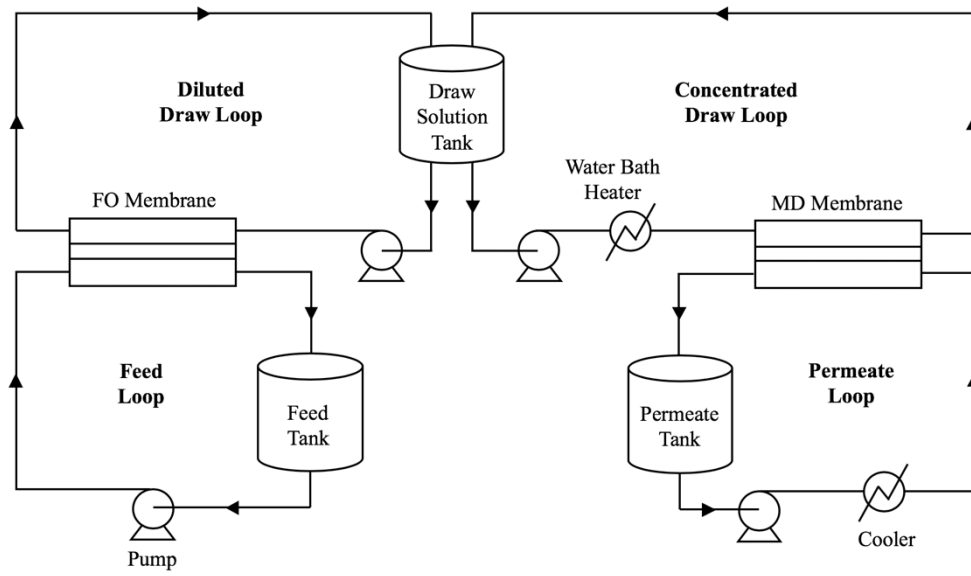


**Fig. 3.** Experimental configuration of FO-MD hybrid system

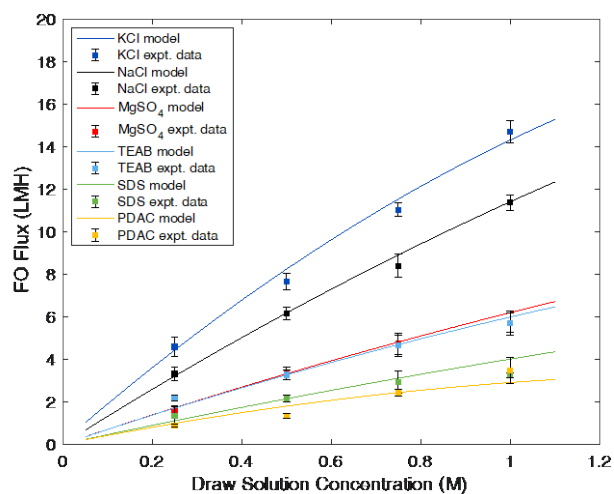
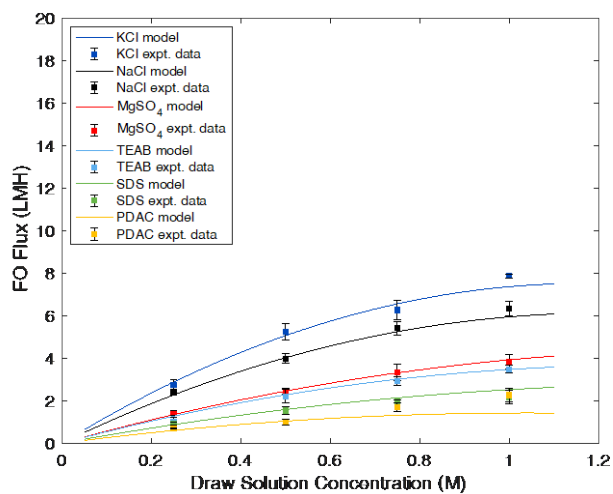


**Fig. 4.** Variation in FO permeate flux with draw solution concentration in (a) AL-FS membrane configuration and (b) AL-DS membrane configuration



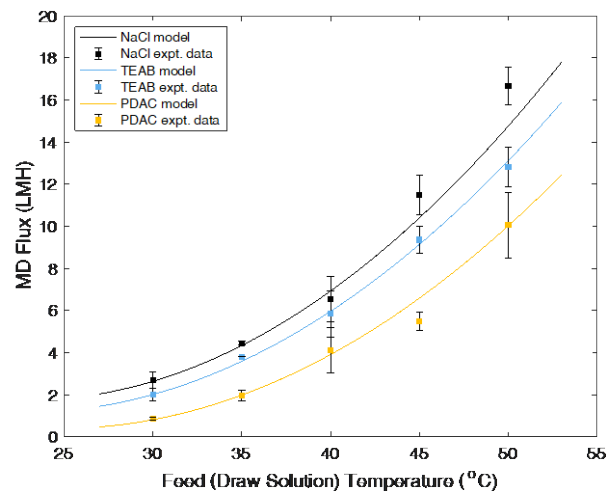


**Fig. 5.** Characterisation of MD permeate flux with feed temperature

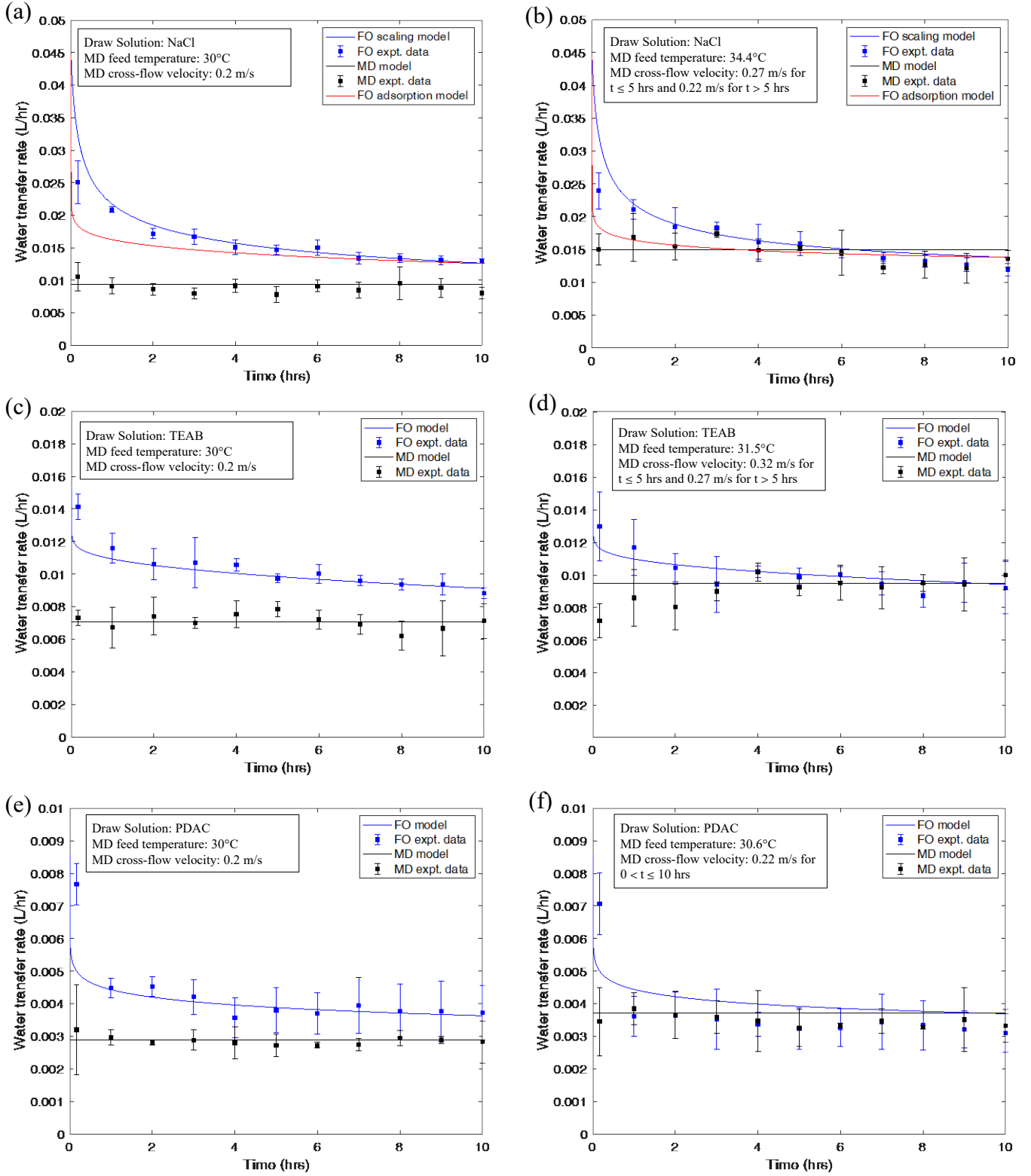


**Fig. 6.** FO-MD hybrid tests for unbalanced systems with draw solutions of (a) NaCl, (c) TEAB and (e) PDAC and balancing test results for (b) NaCl, (d) TEAB and (f) PDAC

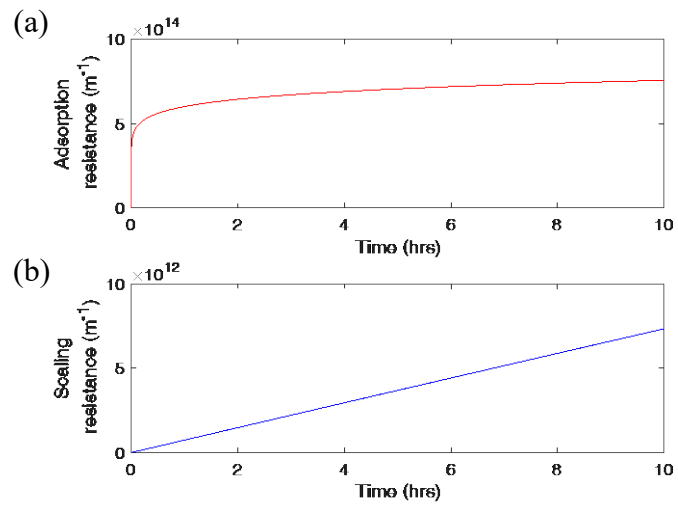


**Fig. 7.** Comparison of (a) adsorption and (b) scaling resistances modelled for NaCl

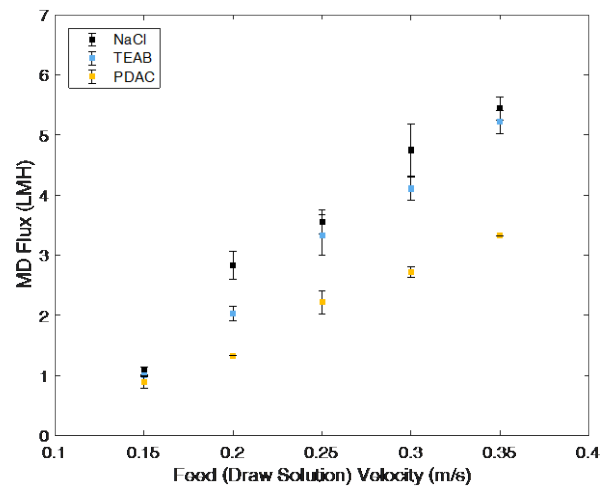


**Fig. 8.** Effect of varying feed cross-flow velocity on MD permeate flux

**Table 1**

Initial conditions applied to FO-MD hybrid system.

	NaCl	TEAB	PDAC
Feed tank concentration (M)	0	0	0
Draw tank concentration (M)	0.5	0.5	0.5
Feed tank volume (L)	0.7	0.7	0.7
Draw tank volume (L)	0.4	0.4	0.4
Permeate tank volume (L)	0.4	0.4	0.4
FO permeate flux (LMH)	6.17	3.26	1.79
MD permeate flux (LMH)	3.14	2.01	0.80

**Table 2**

Properties of FO (AQP), FO (HTI, CTA) and MD (MS) membranes.

	Length (m)	Width (m)	Thickness ( $\mu\text{m}$ )	Pore size (nm)	Water permeability coefficient, A (LMH/bar)	Solute permeability coefficient, B (LMH)	Structural parameter, S ( $\mu\text{m}$ )	Refs.
FO (AQP)	0.1015 <sup>a</sup>	0.041 <sup>a</sup>	110	n.a. <sup>b</sup>	0.52 $\pm$ 0.06	0.09	630	[65]
FO (HTI, CTA)	-	-	30-50	0.74	0.86	0.6	465	[65- 68]
MD (MS)	0.09 <sup>a</sup>	0.04 <sup>a</sup>	160	220	-	-	-	[69]

<sup>a</sup> Dimensions of the membranes used in this study.<sup>b</sup> Pore size of active layer is not available.

**Table 3**

Overview of TEAB, SDS and PDAC draw solutes.

Draw Solute	Type	Charge	Formula	Molecular weight (g/mol)	Critical micelle concentration (M)
TEAB	Surfactant	Cationic	(C <sub>2</sub> H <sub>5</sub> ) <sub>4</sub> NBr	210.16	0.16
SDS	Surfactant	Anionic	C <sub>12</sub> H <sub>25</sub> OSO <sub>3</sub> Na	288.37	0.008
PDAC	Polyelectrolyte	Cationic	(C <sub>8</sub> H <sub>16</sub> NCl) <sub>n</sub>	161.5 <sup>c</sup> 200,000-350,000 <sup>d</sup>	-

<sup>c</sup> represents the molecular weight of each monomeric unit.<sup>d</sup> represents the average molecular weight of PDAC in solution.

**Table 4**

System fouling parameters applied to FO-MD model.

	NaCl (scaling)	NaCl (adsorption)	TEAB	PDAC
$k_{ad}$	-	$6 \times 10^{14}$	$1.1 \times 10^{14}$	$2.4 \times 10^{14}$
$n_{ad}$	-	10	9	7
$k_{sc1}$	$3.7 \times 10^{14}$	-	-	-
$k_{sc2}$	0.002	-	-	-
$c_{sc}$	1	-	-	-



**Table 5** MD operating parameters used in unbalanced and balanced FO-MD hybrid systems.

	MD feed temperature (°C)	MD feed cross flow velocity (m/s) for $0 < t \leq 5$ hrs	MD feed cross flow velocity (m/s) for $5 < t \leq 10$ hrs
<b>Unbalanced FO-MD Hybrid System</b>			
NaCl	30	0.2	0.2
TEAB	30	0.2	0.2
PDAC	30	0.2	0.2
<b>Balanced FO-MD Hybrid System</b>			
NaCl	34.4	0.27	0.22
TEAB	31.5	0.32	0.27
PDAC	30.6	0.22	0.22

**Table 6**

Comparison of balanced and unbalanced FO-MD hybrid system results after 10 hours of operation\*.

	NaCl	TEAB	PDAC
<b>Unbalanced FO-MD Hybrid System</b>			
FO water transfer rate (L/hr)	0.013	0.0088	0.0044
MD water transfer rate (L/hr)	0.008	0.0071	0.0033
FO/MD water transfer rate ratio	1.63	1.24	1.33
<b>Balanced FO-MD Hybrid System</b>			
FO water transfer rate (L/hr)	0.012	0.0092	0.0033
MD water transfer rate (L/hr)	0.014	0.01	0.0031
Increase in permeate production over 10 hours (%)	87.4	62.4	3.3
Increase in MD permeate production relative to FO permeate production over 10 hours (%)	32.8	25.3	35.5

\* Unbalanced and balanced FO-MD operating conditions are given in Table 4.

**Table D1**

Corrected Van't Hoff factor for different draw solutions.

Draw Solution	Corrected Van't Hoff factor ( $\phi$ )
KCl	1.665
NaCl	1.16
MgSO <sub>4</sub>	0.62
TEAB	0.625
SDS	0.4
PDAC	0.41